



**HAL**  
open science

# The Medial Offshore Record of Explosive Volcanism Along the Central to Eastern Aegean Volcanic Arc: 1. Tephrostratigraphic Correlations

S. Kutterolf, A. Freundt, T. H Hansteen, R. Dettbarn, F. Hampel, C. Sievers,  
C. Wittig, S. R Allen, Timothy H. Druitt, J. Mcphie, et al.

► **To cite this version:**

S. Kutterolf, A. Freundt, T. H Hansteen, R. Dettbarn, F. Hampel, et al.. The Medial Offshore Record of Explosive Volcanism Along the Central to Eastern Aegean Volcanic Arc: 1. Tephrostratigraphic Correlations. *Geochemistry, Geophysics, Geosystems*, 2021, 22 (12), 10.1029/2021GC010010 . hal-03554076

**HAL Id: hal-03554076**

**<https://uca.hal.science/hal-03554076>**

Submitted on 3 Feb 2022

**HAL** is a multi-disciplinary open access archive for the deposit and dissemination of scientific research documents, whether they are published or not. The documents may come from teaching and research institutions in France or abroad, or from public or private research centers.

L'archive ouverte pluridisciplinaire **HAL**, est destinée au dépôt et à la diffusion de documents scientifiques de niveau recherche, publiés ou non, émanant des établissements d'enseignement et de recherche français ou étrangers, des laboratoires publics ou privés.



Distributed under a Creative Commons Attribution - NonCommercial - NoDerivatives 4.0  
International License



## RESEARCH ARTICLE

10.1029/2021GC010010

This article is a companion to Kutterolf et al. (2021), <https://doi.org/10.1029/2021GC010011>.

**Key Points:**

- Marine tephrostratigraphy for the Aegean Arc
- Chemical fingerprinting to correlate on and offshore tephras

**Supporting Information:**

Supporting Information may be found in the online version of this article.

**Correspondence to:**

S. Kutterolf,  
[skutterolf@geomar.de](mailto:skutterolf@geomar.de)

**Citation:**

Kutterolf, S., Freundt, A., Hansteen, T. H., Dettbarn, R., Hampel, F., Sievers, C., et al. (2021). The medial offshore record of explosive volcanism along the central to eastern Aegean Volcanic Arc: 1. Tephrostratigraphic correlations. *Geochemistry, Geophysics, Geosystems*, 22, e2021GC010010. <https://doi.org/10.1029/2021GC010010>

Received 6 JUL 2021  
Accepted 14 OCT 2021

**Author Contributions:**

**Conceptualization:** A. Freundt  
**Data curation:** T. H. Hansteen, R. Dettbarn, F. Hampel, C. Sievers, C. Wittig, K. Pank, J. C. Schindlbeck-Belo, K.-L. Wang, H.-Y. Lee  
**Funding acquisition:** A. Freundt, T. H. Hansteen  
**Resources:** S. R. Allen, J. McPhie, P. Nomikou, K.-L. Wang, H.-Y. Lee, B. Friedrichs  
**Visualization:** K. Pank, J. C. Schindlbeck-Belo  
**Writing – review & editing:** A. Freundt, T. H. Hansteen, J. McPhie, P. Nomikou, K. Pank, J. C. Schindlbeck-Belo

© 2021. The Authors.

This is an open access article under the terms of the [Creative Commons Attribution License](https://creativecommons.org/licenses/by/4.0/), which permits use, distribution and reproduction in any medium, provided the original work is properly cited.

## The Medial Offshore Record of Explosive Volcanism Along the Central to Eastern Aegean Volcanic Arc: 1. Tephrostratigraphic Correlations

S. Kutterolf<sup>1</sup> , A. Freundt<sup>1</sup> , T. H. Hansteen<sup>1</sup> , R. Dettbarn<sup>1</sup>, F. Hampel<sup>1</sup>, C. Sievers<sup>2</sup>, C. Wittig<sup>1</sup>, S. R. Allen<sup>3</sup>, T. H. Druitt<sup>4</sup>, J. McPhie<sup>3</sup> , P. Nomikou<sup>5</sup> , K. Pank<sup>1</sup>, J. C. Schindlbeck-Belo<sup>1</sup>, K.-L. Wang<sup>6,7</sup> , H.-Y. Lee<sup>6</sup>, and B. Friedrichs<sup>8</sup> 

<sup>1</sup>GEOMAR Helmholtz Centre for Ocean Research Kiel, Kiel, Germany, <sup>2</sup>Institute for Geology and Paleontology, University of Hamburg, Hamburg, Germany, <sup>3</sup>School of Natural Sciences, University of Tasmania, Hobart, NSW, Australia, <sup>4</sup>CNRS, IRD, OPGC, Laboratoire Magmas et Volcans, Université Clermont Auvergne, Clermont-Ferrand, France, <sup>5</sup>Department of Geology and Geoenvironment, National Kapodistrian University of Athens, Athens, Greece, <sup>6</sup>Institute of Earth Sciences, Academia Sinica, Taipei, Taiwan, <sup>7</sup>Department of Geosciences, National Taiwan University, Taipei, Taiwan, <sup>8</sup>Institute of Earth Science, University of Heidelberg, Heidelberg, Germany

**Abstract** The Milos, Christiana-Santorini-Kolumbo (CSK) and Kos-Yali-Nisyros (KYN) volcanic complexes of the Aegean Volcanic Arc have repeatedly produced highly explosive eruptions from at least ~360 ka into historic times and still show recent unrest. We present the marine tephra record from an array of 50, up to 7.4 m long, sediment cores along the arc collected in 2017 during RV Poseidon cruise POS513, which complements earlier work on distal to ultra-distal eastern Mediterranean sediment cores. A unique set of glass-shard trace element (LA-ICPMS) compositions complements our major element (EMP) data on 220 primary ash layers and 40 terrestrial samples to support geochemical fingerprinting for correlations with 19 known tephras from all three volcanic complexes and with the 39 ka Campanian Ignimbrite from the Campi Flegrei, Italy. The correlations include 11 eruptions from CSK (Kameni, Kolumbo 1650, Minoan, Cape Riva, Cape Tripiti, Upper Scoriae 1 and 2, Middle Pumice, Cape Thera, Lower Pumice, Cape Therma 3). We identify a previously unknown widespread tephra from a plinian eruption on Milos (Firiplaka Tephra). Near the KYN we correlate marine tephras with the Kos Plateau Tuff, the Yali 1 and Yali 2 tephras, and the Upper and Lower Pumice on Nisyros. Between these two major tephras, we found two tephras from Nisyros not yet observed on land. The four Nisyros tephras form a systematic trend toward more evolved magma compositions. In the companion paper we use the tephrostratigraphic framework established here to constrain new eruption ages and magnitudes as a contribution to volcanic hazard assessment.

**Plain Language Summary** The Aegean Volcanic Arc comprises the Milos, Christiana-Santorini-Kolumbo and Kos-Yali-Nisyros volcanic complexes that present particularly high threats for humans and economy due to abundant highly explosive eruptions in the past. The systematic catalog of how eruption products are dispersed on the seafloor (marine tephras) with time provides information on the number and recurrence of eruptions, on their size, and intensities and is thus essential to quantitatively assess future volcanic hazards and risks. During RV Poseidon cruise POS513 in the Eastern Aegean Sea we recovered 50 sediment cores up to 7.4 m long. More than 220 tephra deposits (e.g., volcanic glass shards) from these eruptions were identified. Glass shard compositions from all layers were used for subsequent geochemical fingerprinting to correlate them with 19 known onshore Aegean eruptions as well as with the 39 ka Campanian Ignimbrite eruption from the Campi Flegrei, Italy. Correlations with 11 eruptions from Christiana-Santorini-Kolumbo are established. We identify a previously unknown widespread tephra from an eruption on Milos (Firiplaka Tephra). At the eastern region of the arc, we correlate 7 marine tephras with the Kos-Yali-Nisyros volcanic complex.

### 1. Introduction

The islands of the Aegean Volcanic Arc are a popular travel destination with over 1 million tourists every year but are also locations of strong tectonic and volcanic activity. In the central part of the arc, the entire Christiana-Santorini-Kolumbo (CSK) volcanic complex (Nomikou et al., 2019) as well as Milos Island have been highly active, generating over 100 explosive eruptions from ~360,000 years ago to recent times (Druitt et al., 1999) (Figures 1b

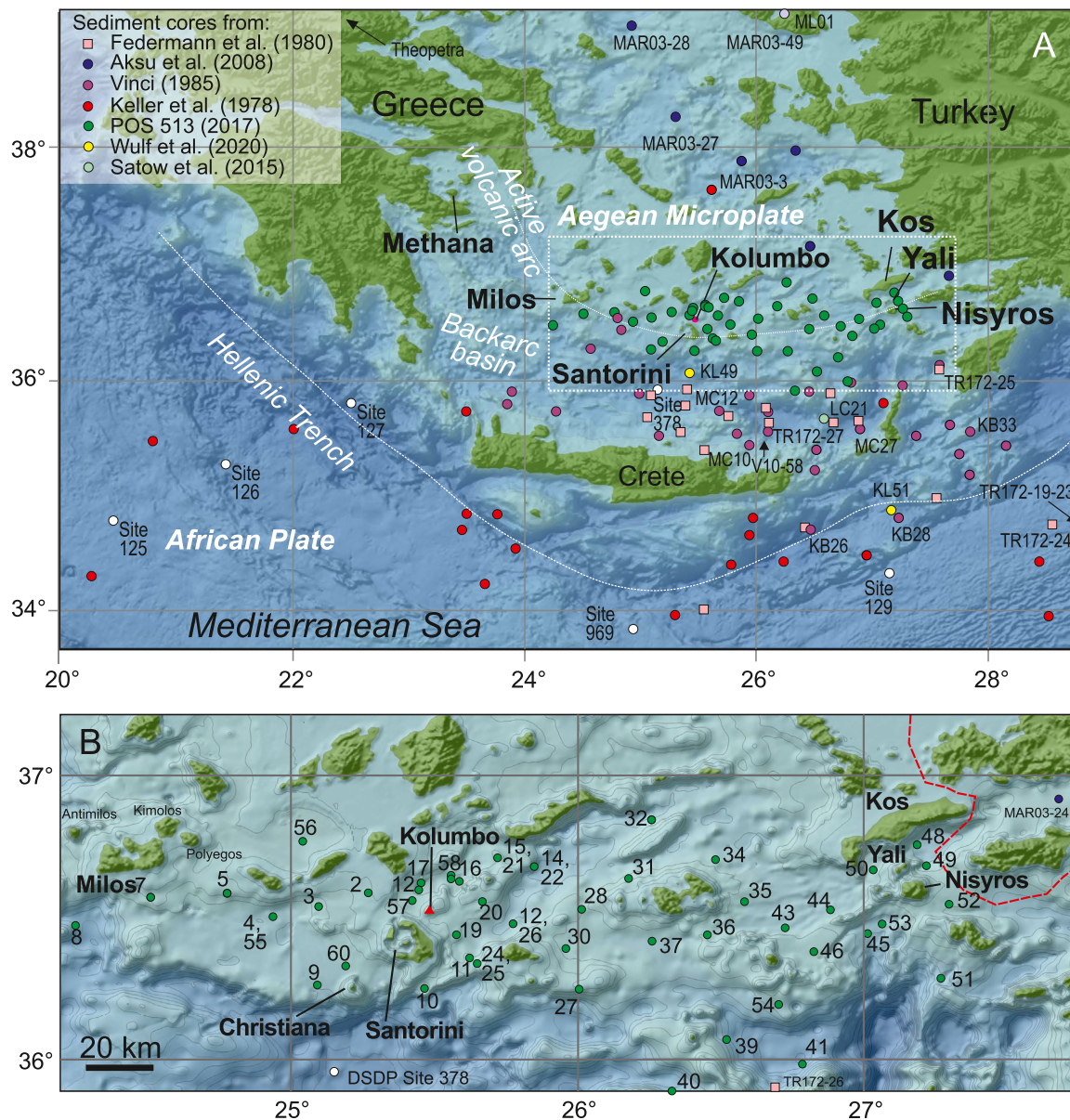


**Figure 1.** (a) Topographic and bathymetric overview map of the Aegean region. Green dots mark the core positions of this study in the region outlined by white-dotted box, that is enlarged in (b). Dots and squares of other colors represent sites of shallow gravity and box coring carried out to date in the Aegean region, white dots indicate deep drilling locations from Ocean Deep Drilling Project expeditions. (b) Close up of our study area in the Central to Eastern Aegean Sea; numbered green circles identify the cores collected during RV Poseidon cruise POS513. Red line is the Greece-Turkey border. Maps created using GeoMapApp (<http://www.geomapapp.org>-GMRT-Global-Multi-Resolution-Topography) (Ryan et al., 2009).

and 2a). Santorini caldera has a well-documented violent eruption history and showed seismic unrest in the years 2011–2012 (Druitt et al., 1999; Newman et al., 2012; Parks et al., 2012; Pyle & Elliott, 2006). Tephra from such large-volume eruptions have been found widely distributed across the Mediterranean seafloor (e.g., Keller et al., 1978; Federman & Carey, 1980; Vinci, 1985; Hardiman, 1999; Wulf et al., 2002, 2020; Aksu et al., 2008, Figure 1a). However, less energetic inter-plinian activity also produced numerous tephras intercalated with major tephras (Vespa et al., 2006), and some of these may also have been emplaced on the surrounding seafloor (Satow et al., 2015; Wulf et al., 2020).

The Kolumbo seamount, 7 km northeast of Santorini, produced a highly explosive eruption in 1650 AD and since then has been hydrothermally and seismically active (Bohnhoff et al., 2006; Carey, Nomikou, Croff Bell, Lilley, et al., 2013; Nomikou, Carey, Papanikolaou, et al., 2012; Sigurdsson et al., 2006).

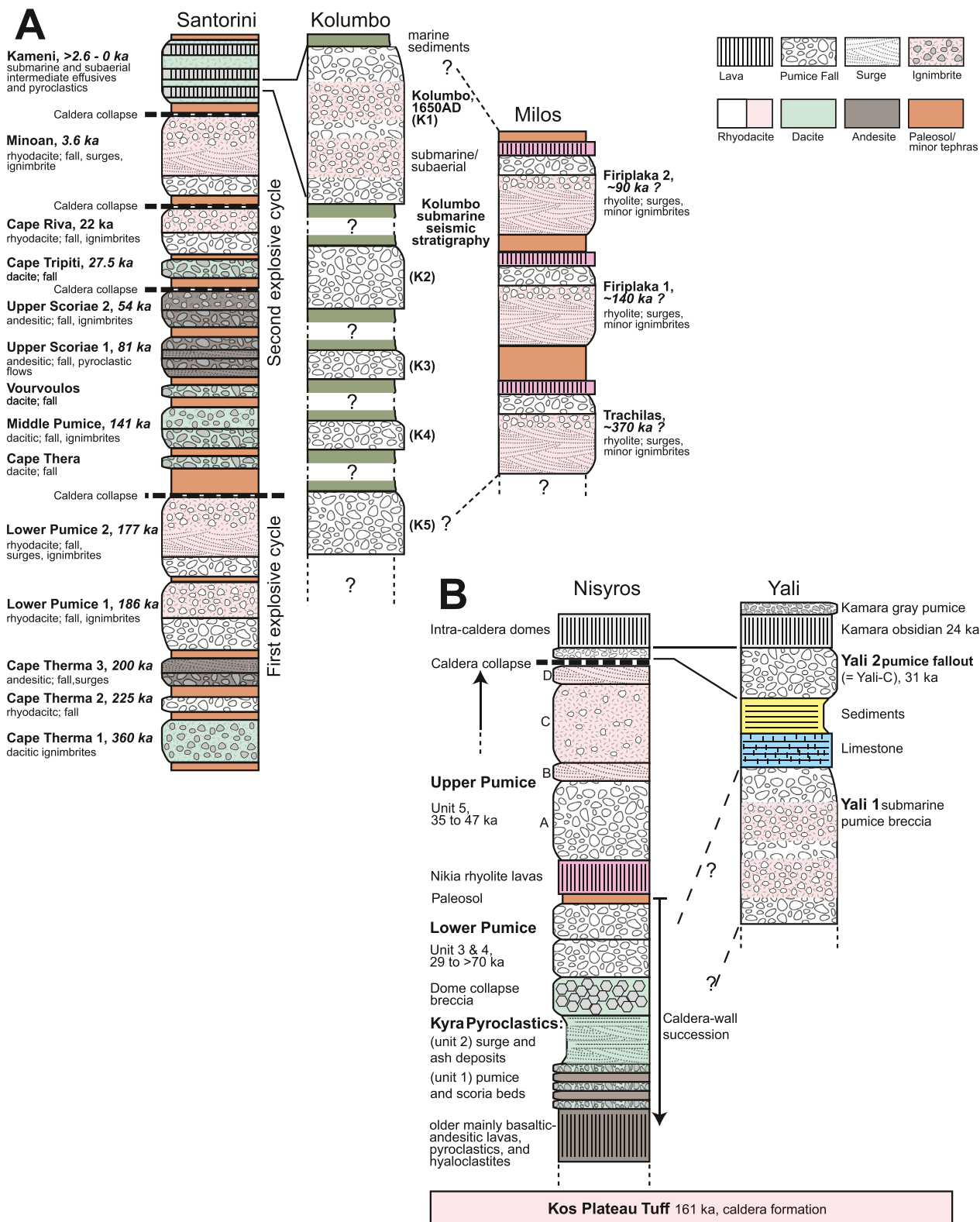


**Figure 2.** (a) Composite stratigraphic profiles (not to scale) of larger pyroclastic deposits on Santorini and preliminary stratigraphies for Kolumbo and Milos. Compiled from Fytikas et al. (1986), Druitt et al. (1999), Stewart and McPhie (2006), Nomikou, Papanikolaou, et al. (2013), and Hübscher et al. (2015). (b) Composite stratigraphic profiles of Nisyros and Yali. Compiled from Limburg and Varecamp (1991), Francalanci et al. (1995), Allen and McPhie (2000), Nomikou, Papanikolaou, and Dietrich (2018).

The younger eruptive history of the Kos-Yali-Nisyros (KYN) volcanic complex at the eastern end of the Aegean Volcanic Arc commenced after the paroxysmal caldera-forming eruption of the Kos Plateau Tuff (KPT) 161 kyrs ago (Allen & Cas, 2001; Allen et al., 1999; Smith et al., 1996). Inside the caldera the two younger volcanic centers of Yali and Nisyros have produced frequent explosive eruptions over at least the last 50 kyrs (Figures 1 and 2b).

The past highly explosive eruptions of all volcanic complexes ranged from submarine to subaerial, including caldera-forming events, which have discharged their volcanic products into adjacent marine basins creating a rich archive of past eruptions. While Santorini has been extensively investigated over the past decades, the stratigraphy and eruptive histories of Milos and the Kos-Nisyros volcanic complex are not fully understood. An improved understanding is important to assess the geohazards for residents, tourists and the environment, and can be gained from the submarine tephra around the islands. Therefore, we make use of the 47 sediment gravity cores of 0.21–7.44 m length as well as three box cores collected during the RV Poseidon cruise POS 513 in the eastern Aegean Sea (Figure 1; Freundt, 2017). Here, we correlate ash layers between these cores and their source volcanoes on land to reconstruct an overall eastern Aegean Sea tephrostratigraphy. This forms the basis for our discussions of new constraints on eruption ages, magnitudes and intensities, as well as the variability of marine sedimentation rates along the Aegean Volcanic Arc, in the companion paper (Kutterolf, Freundt, Druitt, et al., 2021).

## 2. Geological Setting

The Aegean Sea, as a part of the Mediterranean Sea, is characterized by a complex arrangement of subduction zone segments at which the African (Nubian) plate subducts beneath the Eurasian plate. The subduction was initiated in the Miocene (Zhu et al., 2006) and is continuing until today. At the Hellenic trench south of the Aegean Sea, the eastern Mediterranean lithosphere (frontal part of the African plate) subducts with a velocity of  $\sim 4$  cm/yr and a mean dip angle of  $25^\circ$  beneath the continental Aegean microplate, resulting in one of the tectonically most active regions of western Eurasia (e.g., McKenzie, 1972; Papazachos et al., 2005; Shaw & Jackson, 2010). The overriding Aegean continental microplate is part of the Hellenic (Alpine) orogen and is dominated by Early Triassic metamorphic rocks (e.g., Cycladic Blueschists; Bonneau & Kienast, 1982). Slab retreat and rapid southward migration of the Hellenic trench since the Miocene (Zhu et al., 2006) led to extension in the southern and central Aegean region causing deep basins (e.g., the Cretan basin) and seismically active faults as well as horst and graben structures on the Aegean seafloor (Le Pichon & Kreemer, 2010; Royden & Papanikolaou, 2011).

The Aegean Volcanic Arc stretches from the Gulf of Saronikos in the northwest to an area close to the Turkish coast in the East and includes the active volcanic centers at Methana, Milos, Santorini, and Nisyros (Figure 1). The volcanic structures are hosted within extensional neotectonic basins/grabens cross-cutting the Plio-Quaternary sedimentary sequences. The large marginal faults of the basins are typically normal faults locally associated with dextral NE–SW strike-slip zones. The prevailing tectonic orientation is NE–SW at Santorini and Nisyros and NW–SE at Methana and Milos, following the general geometry of the volcanic arc. East-west faults are observed to disrupt the previous arc-parallel NW–SE structures at Methana and Milos (e.g., Piper & Perissoratis, 2003; Nomikou, Papanikolaou, et al., 2013; Nomikou, Hubscher, et al., 2016; Nomikou, Hubscher, Papanikolaou, et al., 2018).

Faults facilitate the ascent of magmas along the active Aegean Volcanic Arc, since the distribution of volcanic centers and the linear alignment of eruptive vents follow fault orientations (Pe-Piper & Piper, 2005). Whereas large, composite volcanoes with caldera structures (Santorini and Kos-Yali-Nisyros) can be found in the central and eastern sectors of the arc, small, commonly monogenetic eruptive centers prevail in the western sector (Francalanci et al., 2005). The similar distance of all volcanoes to a Benioff zone at  $\sim 130$  km depth provides clear evidence for the role of subduction in the genesis of this volcanism (e.g., Papazachos et al., 2005). Accordingly, typical calc-alkaline compositions can be found at all volcanic centers although variations in abundance of different magma types in space and time along the arc can be observed (Pe-Piper & Piper, 2005).

### 3. Active Volcanoes and Their Tephrostratigraphy

#### 3.1. Milos Volcanic Complex

The islands of Milos, Antimilos, Kimolos and Polyegos, form the westernmost volcanic complex in our study area (Figure 1b). The geology of Milos can be divided into four main units: (a) Mesozoic metamorphic basement, (b) Neogene sedimentary rocks, (c) Pliocene and Pleistocene to recent volcanic sequences and (d) the alluvial cover (e.g., Fytikas et al., 1986).

Explosive rhyolitic volcanism on Milos during the Pliocene and Quaternary is documented by a well-exposed succession of pumiceous deposits (Rinaldi & Campos Venuti, 2003). The volcanic activity started at  $2.66 \pm 0.07$  Ma with submarine rhyolitic explosive eruptions before the volcanic activity emerged around  $1.44 \pm 0.08$  Ma and formed scattered subaerial andesitic and dacitic to rhyolitic centers (Fytikas et al., 1986; Stewart & McPhie, 2006). The Pliocene-Recent volcanic sequence of Milos has been subdivided into five units by Fytikas et al. (1986) and further investigated by Stewart and McPhie (2006). It comprises deposits from submarine rhyolitic cryptodomes and pumice cones at the base (unit 1), followed by submarine dacitic and andesitic domes and lavas (unit 2), subsequent submarine to subaerial lavas, domes, and pyroclastic deposits of variable compositions (unit 3), then the rhyolitic lava-pumice complexes of Trachilas and Firiplaka (unit 4), and finally the locally confined deposits from phreatic activity formed until recent times (unit 5). The eruption products cover several square kilometers on the island and include pyroclastic sequences up to  $\sim 200$  m thick and small-volume, biotite and quartz bearing rhyolite lavas up to 100 m in thickness (Figure 2; Fytikas et al., 1986; Campos Venuti & Rossi, 1996; Stewart & McPhie, 2006).

#### 3.2. Christiana-Santorini-Kolumbo Volcanic Complex

The Christiana-Santorini-Kolumbo (CSK) volcanic complex is located in the central sector of the 450-km-long Aegean Volcanic Arc (Figure 1) and comprises three distinct volcanic centers along a 40-km-long,  $040^{\circ}$ – $045^{\circ}$  striking fault zone (Nomikou, Papanikolaou, et al., 2013; Nomikou, Carey et al., 2013), crossing the island arc. At the SW end of this zone and 23 km from Santorini lies the extinct Christiana Volcano with its two main islets Askani and Eschati reaching up to 283 m above the sea level. Christiana Volcano has produced lavas and tuffs of unknown ages (Aarbourg & Frechen, 1999).

Santorini at the center of the CSK complex has produced volcanic deposits since the Mid-Pleistocene that overlie the Mesozoic to Tertiary basement (Jackson, 1994). The Santorini volcanic center consists of the islands Thera, Thirasia and Aspronisi that are arranged as a dissected ring around a flooded caldera. The caldera, a  $11 \times 7$  km composite structure, resulted from at least four collapse events over the last 200 kyrs and contains in its center the post-caldera volcanic islands Palea Kameni and Nea Kameni (Druitt & Francaviglia, 1992; Pyle & Elliott, 2006; Nomikou et al., 2014). The oldest dated volcanic rocks are early Quaternary submarine tuffs near Akrotiri in SW Thera, which are speculated to originate from vents at Akrotiri and Christiana (Francalanci et al., 2005). Subaerial volcanism at Santorini began about 650 ka ago (Druitt, 2014; Druitt et al., 1999), and has continued until the present day. More than a hundred explosive eruptions within the last 250,000 years, triggering at least four caldera collapses, make Santorini one of the world's most active arc volcanoes (Druitt et al., 1999). The succession of major tephra events, including at least 12 large plinian eruptions, is summarized in Figure 2. This succession has been interpreted to represent two cycles ( $\sim 170$  ky per cycle) of increasing eruption intensities and magnitudes, one from Cape Therma 1 to Lower Pumice 2, and the other from Cape Thera to the Minoan eruption (Druitt et al., 1989). Each cycle started with eruptions of mostly intermediate-composition magmas and developed to large silicic eruptions at the end.

The last caldera collapse was caused by the late Bronze Age (3.6 ka) Minoan eruption (Druitt, 2014), which discharged several tens of  $\text{km}^3$  DRE (Johnston et al., 2014; Pyle, 1990) of rhyodacitic magma, distributed ash over a large area of the eastern Mediterranean and Turkey, and generated tsunamis that may have contributed to the downfall of the advanced Minoan civilization (e.g., McCoy & Heiken, 2000; Nomikou, Druitt, et al., 2016; Vougioukalakis & Fytikas, 2005). After the Minoan eruption, volcanic activity continued inside the caldera where effusive and mildly explosive eruptions built up the dacitic Palea Kameni and Nea Kameni islands between 197 BC and 1950 AD (Nomikou et al., 2014).

About 7 km off the north-eastern coast of Thera, the ~480-m high submarine Kolumbo Volcano and 23 other submarine cones formed within the fault-bordered Anydros basin (Nomikou, Carey, Papanikolaou, et al., 2012; Nomikou, Papanikolaou, et al., 2013; Nomikou, Carey et al., 2013; Nomikou, Hübscher, et al., 2016). Seismic profiles across Kolumbo revealed a complex internal structure of five volcanoclastic units (Figure 2) probably due to repeated phases of construction and destruction (Hübscher et al., 2015; Hoofstede et al., 2017; Nomikou et al., 2019). In 1650 AD the Kolumbo Volcano exploded in a paroxysmal event which ejected huge quantities of volcanic ash, forming a 1.7-km-diameter summit crater (Carey, Nomikou, Croff Bell, & Ballard, 2013; Nomikou, Carey, Papanikolaou, et al., 2012), and generating a devastating tsunami (Nomikou, Carey, Croff Bell, et al., 2012; Ulvrova et al., 2016). This event was the most hazardous and powerful eruption in the Greek territory in historic times killing more than 70 people on Thera and causing damages within a radius of 150 km (Fouqué, 1879; Vougioukalakis & Fytikas, 2005). The submarine to emergent rhyolitic pumice deposits are ~250 m thick in the crater walls whereas distal fall deposit is found as far away as on the Turkish mainland and forms the youngest widespread ash layer on the regional seafloor. Cantner et al. (2014) investigated the stratigraphy of the proximal submarine deposits and the pre-eruptive storage conditions of the rhyolitic magma, and concluded that the explosive eruption started submarine but finally emerged above the sea surface. Fuller et al. (2018) sampled and analyzed the fine-grained ash deposits on the seafloor around Kolumbo which form a strong contrast to the fines-poor breccias found at the crater. The fine-grained ash deposits were emplaced by various forms of vertical and lateral ash-rich gravity currents. Today, the shallowest point of Kolumbo Volcano lurks only 18 m below sea level, and there is continuing CO<sub>2</sub> degassing and hydrothermal activity in the north-eastern part of the crater (Carey, Nomikou, Croff Bell, Lilley, et al., 2013; Kiliyas et al., 2013). The hydrothermal vent field north of Kolumbo, discovered in 2006 by Sigurdsson et al. (2006), developed in the latest Pleistocene mainly during explosive events (Hübscher et al., 2015).

### 3.3. Kos-Yali-Nisyros Volcanic Complex

The Kos-Yali-Nisyros volcanic complex (KYN) is located at the eastern end of the Aegean Volcanic Arc and its volcanic activity reaches back to about 3 Ma (e.g., Allen & Cas, 2001; Bachmann et al., 2012). The island of Kos is covered by the Kos Plateau Tuff, product of the largest eruption in the upper Pleistocene ( $161.3 \pm 1.1$  ka; Smith et al., 1996) in the Aegean region.

The vent for the paroxysmal caldera-forming KPT phreatoplinian eruption lies somewhere between the islands of Kos, Yali and Nisyros, and ejected an initial fall deposit and subsequent huge pyroclastic density currents that traveled over the sea and emplaced thick ignimbrites on Kos and other islands (Allen and Cas, 1998, 2001). Six major stratigraphic units have been identified, including a widespread vitric ash fall deposit at the base, followed by several phreatomagmatic surge-like pyroclastic density current deposits and ignimbrites extending up to ~160 km radially from the volcano (Allen et al., 1999). About 60 km<sup>3</sup> DRE of rhyolitic magma were erupted and are thought to have triggered subsidence of a submarine caldera south of Kos (Allen et al., 1999; Nomikou, Papanikolaou, et al., 2013). Subsequently, this structure was re-filled by the Nisyros composite volcano (e.g., Limburg & Varecamp, 1991), the Yali pumice cone (Allen & McPhie, 2000) and the Pleistocene-Recent Strongyli basaltic andesite cone as well as several submarine volcanic cones, which all have formed under strong tectonic control in the complex horst and graben structure (Nomikou, Carey, et al., 2013; Nomikou & Papanikolaou, 2011; Papadopoulos et al., 1998; Papanikolaou & Nomikou, 2001; Tibaldi et al., 2008).

Nisyros Island (8 km diameter) lies south-southeast of Kos Island. Nisyros Volcano grew on a basement of Mesozoic limestones and Neogene sediments and has a 4-km-wide and 450-m-deep caldera as well as 700-m-high post-caldera domes of Late Pleistocene age (Francalanci et al., 1995). The volcanic edifice formed in two cycles of explosive and effusive eruptions fed initially by calc-alkaline basaltic-andesitic and subsequently by rhyolitic magmas (Figure 2b; Volentik et al., 2002; Longchamp et al., 2011; Tomlinson et al., 2012; Dietrich & Lagios, 2018). The first cycle started as a basaltic-andesitic submarine volcano which later emerged and effusively and explosively discharged basaltic-andesites to rhyolites (Kyra pyroclastics and dome collapse breccia, Figure 2). The second cycle started with two major caldera-forming plinian eruptions that destroyed the pre-existing volcano and emplaced the Lower and Upper Pumice layers, each followed by post-caldera dome and lava extrusion as well as erosion and paleosol development after the Lower Pumice (Figure 2; Francalanci et al., 1995; Hardiman, 1999). Finally, Nisyros was covered by the Yali 2 pumice fall deposit. A major issue with the Nisyros

stratigraphy is that published radiometric ages of some deposits vary strongly and do not fit the observed stratigraphic succession (see also part 2 as well as Volentik et al., 2002; Tomlinson et al., 2012; Popa et al., 2020).

Yali Island is located 10 km south of the island of Kos and 5 km north of Nisyros (Figure 1) and lies within an extensional setting (the Kerme Graben; Dewey & Sengör, 1979) and close to or inside the postulated Kos Plateau Tuff caldera (Allen & Cas, 2001; Keller et al., 1990). Yali is the source of the youngest highly explosive eruption of the Kos-Nisyros-Yali volcanic complex, which emplaced the Yali-2 (or Yali-C) subaerial pumice fall deposit ~31 kyrs ago (Figure 2b; Allen & McPhie, 2000). This deposit is locally covered by the 21 ka Kamara obsidian lava and pumice deposit. Yali-2 overlies bioclastic sandstone and limestone units that cover the >150 m thick Yali-1 submarine pumice breccia succession of yet unknown age and hidden basal contact (Allen & McPhie, 2000). The various facies of the Yali-1 tephra formed during submarine eruptions and resulted from deposition of pumice clasts from aqueous suspension, emplacement of submarine gravity currents and re-sedimentation of primary tephra (Allen & McPhie, 2000).

#### 4. Previous Offshore Tephrostratigraphic Work

Given the relatively small size of the Aegean volcanic islands, even moderate size explosive eruptions on land can be expected to produce deposits on the surrounding seafloor. Since plinian eruptions inject volatiles and ash into the stratosphere their dispersal is mainly controlled by the dominantly strong (up to >60 km/hr) westerly stratospheric winds in the Aegean region. These winds transport the eruption products preferentially towards the east-southeast during most of the year (e.g., monthly record of stratospheric winds (18–27 km height) for the last five years; <https://earth.nullschool.net/about.html>). Exceptions occur in the summer months May to August, when northerlies to southerlies are present at moderate strength (5–30 km/hr). Such winds may be an explanation for observed tephra dispersal to the north. Additionally, the tropospheric wind regimes are very variable throughout the year (e.g., Tyrlis & Lelieveld, 2013) and may have influenced the ash dispersal of smaller eruptions as well as specific tropospheric phases (e.g., co-ignimbrite plumes) of large eruptions. The sediments of the Aegean Sea and the central to eastern Mediterranean Sea, (hemi-)pelagic sediments periodically interrupted by sapropels representing periods of deep-sea anoxia (Rohling et al., 2015), therefore contain abundant visible tephra and invisible cryptotephra from the Aegean Volcanic Arc but also from Italian and Anatolian volcanoes. The marine tephrostratigraphy of the Mediterranean Sea is a well-established grid of widely dispersed marker tephra layers that have been subdivided into foraminifera zones from V to Z (e.g., Federman & Carey, 1980; Keller et al., 1978; McCoy, 1981). Thus, tephra layers have been named for example, Z2 (Minoan), Y2 (Cape Riva), X1 (Upper Scoriae 1), or W3 (Kos Plateau Tuff). The advantage of the Mediterranean marine tephrostratigraphy over many other arc regions is that the different deposits and source volcanoes can be reliably distinguished by geochemical compositions (e.g., Aksu et al., 2008; Federman & Carey, 1980; Hardiman, 1999; Karkanis et al., 2015; Keller et al., 1978; Margari et al., 2007; Narcisi & Vezzoli, 1999; Tomlinson et al., 2015, 2012; Vinci, 1985; Wulf et al., 2020, 2002). The major element compositions of Italian alkaline and peralkaline volcanic rocks differ significantly from calc-alkaline products of the Aegean Arc and Anatolian arc volcanoes (e.g., Clift & Blusztajn, 1999). The available geochemical data base for late Quaternary tephra is particularly detailed, especially for Italian volcanic centers (Wulf et al., 2004, 2008, 2012; Tomlinson et al., 2012, 2015) but also for some volcanoes in the Aegean Sea (Satow et al., 2015; Tomlinson et al., 2015; Wulf et al., 2020). However, so far only the largest and most widespread tephra of the Aegean Volcanic Arc have been included in this database. This deficiency was also noted by Wulf et al. (2020) and is particularly relevant for this study because we expect to find tephra from inter-plinian activity, at least from Santorini, in addition to the medial deposits from the large eruptions, because our cores are located at proximal to medial distances from the volcanic islands.

#### 5. Methods

##### 5.1. Marine Core Sampling and Logging

During RV POSEIDON cruise POS 513 (2017), 47 gravity cores and three box cores were recovered between Milos in the west and Kos in the east (Figure 1b). Recovered core length varied between ~30 cm and 7.5 meters (box cores 10–40 cm) at water depths of ~100 to ~1,200 meters (Freundt, 2017).

Visual core descriptions were completed on board using the IODP description scheme from Mazzullo and Graham (1988). The archive-half sections of the sediment cores were visually described for lithologic and sedimentary

features aided by 20× wide-field hand lens and binocular microscope. Visual inspection and smear slide analysis yielded information about variations in lithologic components, color, sedimentary structures, and occasionally drilling disturbances. Lithologic components comprise tephra particles (glass, minerals) as well as various rock fragments and microfossils. For tephra analysis we sampled suspected ash layers on board and enriched the volcanic components from mixed sediment in the laboratory by wet sieving into 63–125 μm and >125 μm fractions. The grain-size fractions were then used for geochemical microanalyses.

## 5.2. Primary Versus Reworked Ash and Ash Pods

Pyroclasts can be incorporated into marine sediments by a variety of processes. These processes include (a) water-settled primary fall emplaced on the seafloor either by settling of single particles or by vertical density currents released from ash concentration zones at the ocean surface, (b) eruption-fed submarine density currents formed either by submarine eruptions or by subaerial pyroclastic density currents entering the ocean, and (c) submarine density currents that entrain and re-deposit pyroclasts (e.g., Cassidy et al., 2014; Freundt et al., 2021; Hopkins et al., 2020; Schindlbeck et al., 2013; Schneider et al., 2001).

We use a combination of criteria to distinguish ash produced by explosive eruptions, herein referred to as “primary,” from “secondary” volcanoclastic deposits emplaced by reworking of primary tephra (see Freundt et al. (2021) for more extensive discussion). Heterogeneous glass-shard compositions that do not show a clear magmatic differentiation trend have been excluded from the final data set. On the other hand, massive or size-graded deposits composed of glass shards of homogeneous compositions are considered primary deposits from explosive eruptions, regardless of the details of final transport and deposition.

Ash pods, that is, isolated lensoid or irregularly shaped bodies of ash in marine sediments, can be formed by a variety of processes but bioturbation and resedimentation of marine ash deposits, sometimes nearly instantaneous, are the most common (Cambray et al., 1993; Fujioka, 1986; Hunt & Najman, 2003). Where ash pods of homogeneous glass composition are arranged in an ash-pod layer, it is reasonable to assume that this layer marks the position of the original primary ash layer. Single ash pods, however, can occur in a position significantly above or below the position of the original ash layer, depending on the mechanism and timing (syn- or post-depositional) of their formation. Single ash pods were not included in the database.

## 5.3. Chemical Analyses

For comparison with marine tephra glass-shard compositions we established a glass-compositional reference data base for Aegean arc tephra using samples from all relevant tephra units that have been stratigraphically well defined by previous studies (Allen & Cas, 1998; Allen & McPhie, 2000; Cantner et al., 2014; Druitt et al., 1999) or by own field work (e.g., Milos, Kolumbo) (see Table S1 for available sample coordinates and Table S2a in Data Set S1 for sampled respective stratigraphic units and geochemical data). The tephra samples have been collected by authors of those studies and come from Milos and Kolumbo (sampled by Nomikou and colleagues), from Santorini (sampled by Druitt and colleagues), and from Kos, Nisyros and Yali (sampled by Allen and McPhie). Samples from Santorini are from near-vertical cliffs and we therefore recommend to refer to the geological map and/or contact T. Druitt for details of sampling sites in order to avoid sampling errors. We crushed samples from all major tephra on land to obtain glass fragments that we analyzed by the same methods as the marine glass shards. The 63–125 μm fraction of both types of samples was embedded with epoxy resin into 12 pre-drilled holes in acrylic mounts and polished to facilitate measurements with the electron microprobe (EMP) and the Laser Ablation Inductively Coupled Plasma Mass Spectrometer (LA-ICP-MS).

### 5.3.1. Electron Microprobe (EMP) Analyses

Glass shards (~7,000 in total) were analyzed for major and minor elements on 474 epoxy embedded samples using a JEOL JXA 8200 wavelength dispersive EMP at GEOMAR, Kiel, utilizing the methods of Kutterolf et al. (2011). A calibrated measuring program was used based on international standards with a 10 μm electron beam to minimize sodium loss. Oxide concentrations were determined using the ZAF correction method. Accuracy was monitored by two measurements each on Lipari obsidian (Lipari rhyolite; Hunt & Hill, 2001) and Smithsonian basaltic standard VGA99 (Makaopuhi Lava Lake, Hawaii; Jarosewich et al., 1980) after every 60 single glass shard measurements (~15 per sample). Standard deviations are <0.5% for major and <10% for minor

elements (with the exception of  $P_2O_5$  and  $MnO_2$  in samples  $>65$  wt%  $SiO_2$ ). All analyses with totals  $>90$  wt% were normalized to 100% in order to eliminate the effects of variable post-depositional hydration and minor deviations in focusing of the electron beam. The acceptable analyses of each sample were then averaged in order to characterize the elemental compositions of each tephra. Layers with heterogeneous compositions but inside differentiation trends were included with their intra-sample deviation in the data base whereas widely heterogeneous compositions outside any possible differentiation trend were excluded. All of the resulting major and trace element data and their respective errors are listed in Tables S2 and S3a in Data Set S1.

### 5.3.2. Laser Ablation-Inductively Coupled-Mass Spectrometry (LA-ICP-MS)

The trace element concentrations of  $\sim 1,500$  glass shards from marine and onland tephtras (150 samples,  $\sim 5$  shards per sample) were determined by LA-ICP-MS between September 2018 and March 2021 at the Academia Sinica in Taipei, Taiwan, providing the first complete trace element reference data base for Aegean arc tephtras. The LA-ICP-MS instrumentation comprises a 193 nm excimer laser (Teledyne CETAC Analyte G2) set to a spot size of 24–30  $\mu m$  (using 5–10  $J/cm^2$  energy density at 4–10 Hz repetition rate), coupled to a high-resolution ICP-MS (Agilent 7900). Detailed machine setups, procedures, and methods of the laboratories are described in Schindlbeck et al. (2016). Following 45 s of blank acquisition, typical ablation times were around 75 s. Data reduction was performed using Version 4.0 of “real-time on-line” GLITTER© software (van Achterberg et al., 2001), immediately following each ablation analysis. Individual silica and calcium concentrations, measured by EMP on the same glass shards, were used as an internal standard to calibrate each trace element analysis. An international glass standard (BCR-2g) was measured every 10 sample measurements in order to monitor accuracy and to correct for matrix effects and signal drift in the ICP-MS, and also for differences in the ablation efficiency between sample and reference material (Günther et al., 1999). The concentrations of NIST SRM 612, needed for external calibration, were taken from Norman et al. (1996). The limit of detection (LOD) for most trace elements was generally  $<100$  ppb. For Rare Earth Elements (REE), the LOD is generally around 10 ppb. The analytical precision is generally better than 10% for most trace elements.

### 5.3.3. Correlation Techniques

Ash-layer correlations are based on glass-shard compositions, supplemented by modal compositions (e.g., crystals, lithic fragments, micro- and macrofossils), sedimentary structures, stratigraphic relationships and geographic location. Supporting data include the shape, vesicularity and vesicle texture of glass shards and pumiceous fragments, and also the mineral content of the ash layers as determined in smear slides (Figures 3 and 4). In order to correlate marine ash beds with tephtras on land, we analyzed the glass compositions of  $>3$  juvenile clasts from one to four different units and/or samples of 24 onshore tephtras at all relevant eruptive centers and complemented these analyses with published data.

The first step in onshore-offshore correlations is the graphical comparison of the average compositions of each marine ash bed with the compositional fields defined for the onshore tephtras. A correlation is accepted when these compositions overlap within the respective analytical errors in all variation diagrams that usefully discriminate tephtra glass compositions. Next to major and trace element concentrations, this approach uses trace element ratios that minimize the influences of both analytical errors and alteration.

The second step is the application of a hierarchical cluster analysis (HCA; e.g., Kutterolf et al., 2008) using Origin 2021 to statistically constrain correlations within a combined marine and onshore tephtra data base. This step is particularly useful where visual inspections of core-to-core and offshore-onshore in the first step remained ambiguous. The HCA creates different cluster solutions between 1 (all samples in one cluster) and  $n$  (each sample in a single cluster) based on the parameters applied to the modeling and the data set. The result of each modeling is a dendrogram, a graphical summary of the cluster solution. Before applying the cluster analysis, we reduced the compositional variables (major and trace elements as well as trace element ratios) by performing a principal component analysis that reduces the variables to 10 components which account for 96.57% of the variance in the samples. We used the nearest and farthest neighbor linkage as well as the Ward clustering method and the single and squared Euclidian distance measuring intervals to test and achieve the best possible correlations for our data set that features both a large compositional variety among the investigated tephtras and small differences for some tephtras from the same eruptive center. Several HCA's were carried out, compared and evaluated with regard to the observed stratigraphic relationships. The Ward clustering method in combination with a squared Euclidian distance measure were the most reliable cluster solutions for the grouping and correlation of the studied samples.

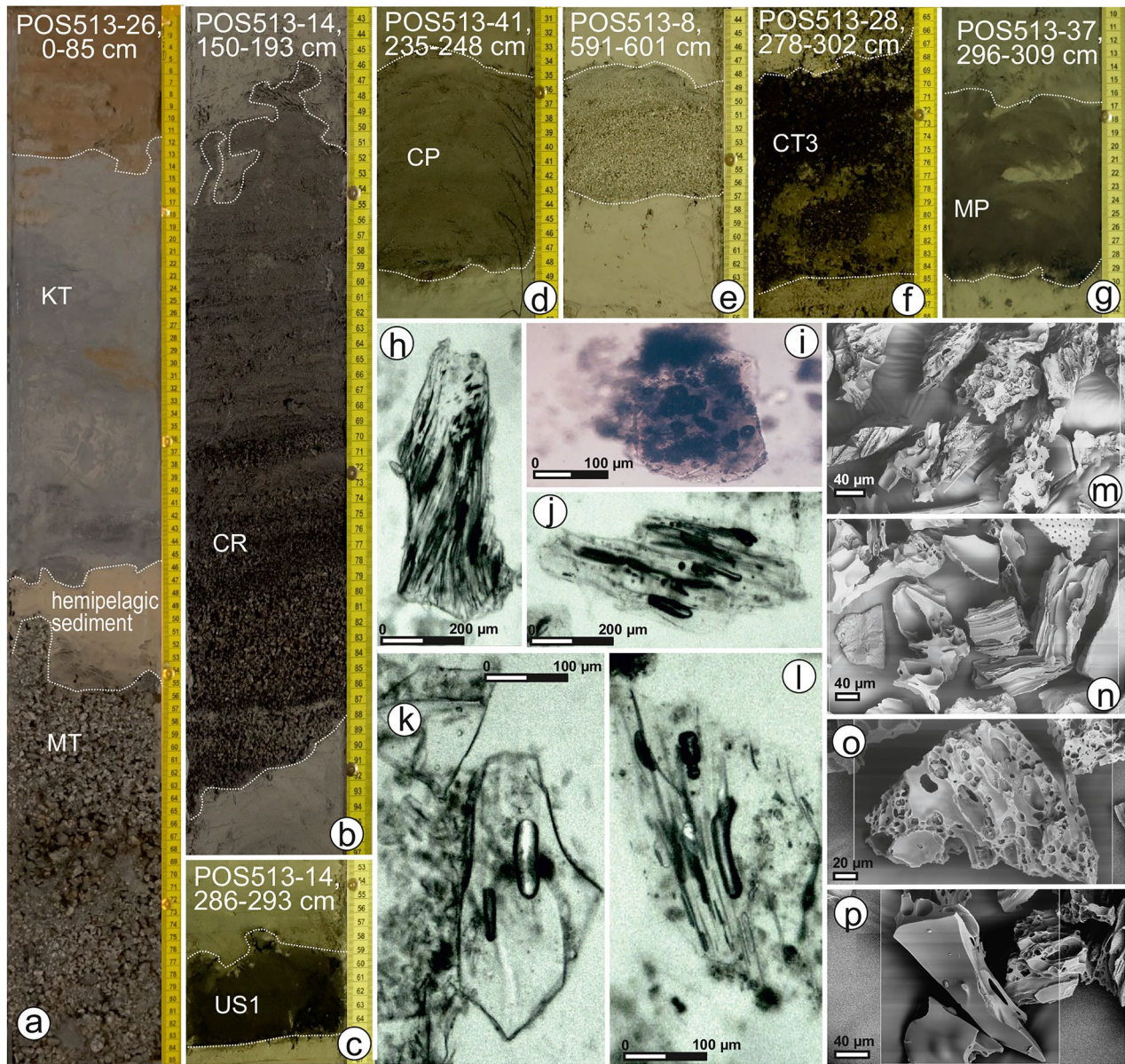


**Figure 3.** Photographs of selected ash layers, smear-slide and backscatter SEM microphotographs of glass shards from Milos and the CSK volcanic complex, showing typical appearance of ash layers and glass-shard textures. (a) Proximal CA3 correlated to Minoan tephra (MT, fine to medium lapilli) and CA1 correlated to Kolumbo tephra (KT, fine to coarse ash) with erosive boundaries. (b) Proximal CA4 correlated to Cape Riva tephra fining upward from fine lapilli, showing stratification and discordant base. (c) Distal massive fine black ash layer CA15, equivalent to Upper Scoriae 1 on Santorini. (d) Massive ash layer CA8 correlated with the Campanian ignimbrite, graded from fine to very fine ash to background sediment. (e) Normally graded fine lapilli to coarse ash layer of unknown tephra with sharp basal and top contacts. (f) Slightly disrupted inversely graded coarse ash to fine lapilli layer of CA20, equivalent to Cape Therma 3, Santorini. (g) Normally graded, medium to very fine ash CA16 correlated with Middle Pumice, Santorini, bioturbated at the top. (h) Twisted fine-textured tubular pumice of CA3 correlated with the Minoan eruption (POS513-26, 75 cm). (i) Blocky glass shard with round vesicles from CA15, correlated with Upper Scoriae 1 (POS 513-37, 227 cm). (j) and (k) Glass shard with few elongated vesicles from CA5, correlated with Cape Tripiti (POS 513-15, 237 cm). (l) Blocky glass shard from CA1, correlated with the 1650 AD Kolumbo eruption (POS 513-26, 42 cm). (m) Pumice fragments with elongated and round vesicles from CA3, correlated with the Minoan tephra (POS 513-21, 18 cm). (n) Cusped and pumiceous glass shard assemblage from CA1, correlated with the 1650 AD Kolumbo eruption (POS 513-16, 45 cm). (o) Pumice with larger elongated and smaller round vesicles from CA1, correlated with the 1650 AD Kolumbo eruption (POS 513-16, 45 cm). (p) Blocky glass shard with very few vesicles from CA1, correlated with the 1650 AD Kolumbo eruption (POS 513-16, 30 cm).

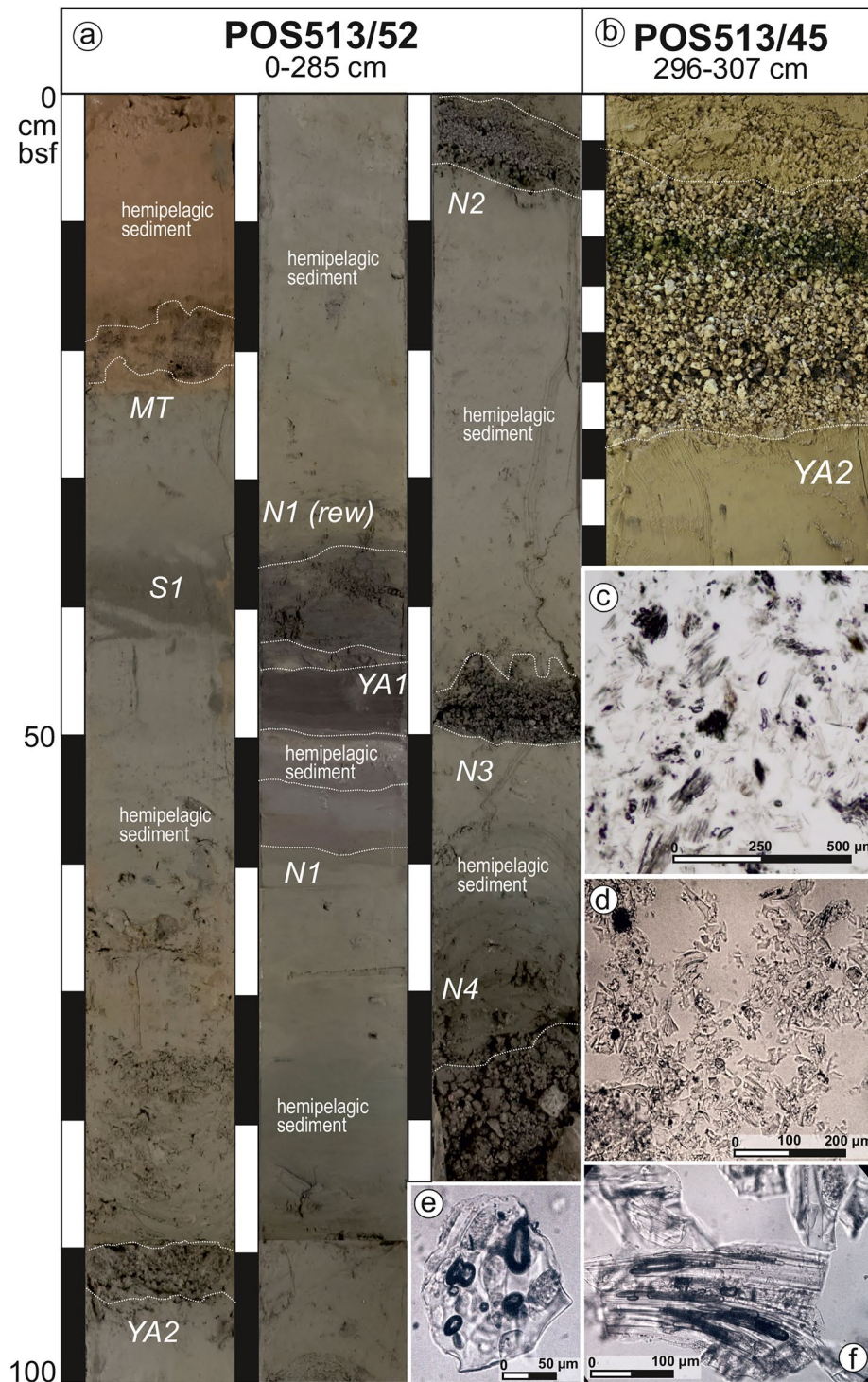


**Figure 4.** Photographs of selected ash layers and smear-slide microphotographs of glass shards from the KYN volcanic field, showing typical appearance of ash layers and glass-shard textures. (a) Sequence of fine (fine to coarse ash) and coarse (fine to medium lapilli) tephra layers in core POS 513–52 showing all identified tephra of Yali and Nisyros volcanoes; MT = Minoan Tephra, YA2 = Yali 2 fall deposit, YA1 = Yali 1 tephra, N1 = Upper Pumice, N2, N3 = intermediate Nisyros tephra, N4 = Lower Pumice. (b) Normally graded fine lapilli to coarse ash layer CA6a correlated with Yali 2 fall deposit; black and greenish layers in the lower and upper parts are lithic enriched. (c) Glass shard assemblage of CA11, correlated to Nisyros 1, showing a mixture of highly vesicular, commonly tubular pumices and cusped to blocky glass shards (POS513-45, 514 cm). (d) Mixture of blocky, cusped and some tubular glass shards from CA6b (POS513-44, 504 cm). (e) example of a less vesicular glass shard with elliptical vesicle from CA11 equivalent to Nisyros 1 (POS513-45, 514 cm). (f) curved tubular pumice fragment from CA14 correlated to Nisyros 4 (POS513-39, 457 cm).

The combination of different discrimination diagrams in combination with HCA, observed stratigraphic order, and ages has the potential to result in unambiguous correlations. In the end, ash layers in single cores that can be correlated across different sites and/or with tephra on land are grouped as a “tephra layer” and are named from young to old (CA 1–20). Thus, a “tephra layer” includes all ash layers in different cores that have been emplaced by the same single volcanic eruption.

## 6. Results

### 6.1. General Description of Cores

The hemipelagic background sediment is composed of layers in the dm-thickness range that consist of clay to silty sand and volcanoclastic clay to sand. Coarser sediments (sand to granule) are dominated by bioclasts like foraminifera, nannofossils, sponge spicules, and echinoderms mixed with some phyllosilicate minerals; clays and silty clays contain foraminifera and nannofossils. Overall volcanoclastic matter and reworked sedimentary clasts (consolidated clay and silt agglomerates) are strongly admixed in the background sediment.

The cores collected in the central and eastern Aegean Sea contain a total of 348 ash/lapilli bearing horizons, which occur as primary ash layers, ash pod horizons, ash pods and dispersed ash. They are intercalated within the hemipelagic sediment and range from 1 to 65 cm in thickness (Figures 3 and 4). Sorting out reworked tephra-bearing layers and combining multiple beds within the same layer, we classify the remaining 220 ash layers as primary pyroclastic deposits. These include 149 pale gray to white felsic tephra, 54 gray beds of probably intermediate composition and 17 black layers of mafic compositions (e.g., Figures 3 and 4).

The upper boundaries of the tephra layers are commonly irregular, horizontal to inclined, and either sharp or gradational with the overlying sediment. The lower boundaries are predominantly very sharp, horizontal to inclined, and locally show features of erosive cutting into the underlying hemipelagic sediments, creeping or slumping (Figures 3a–3f). Load casts are found especially where coarser ash to lapilli overlie fine sediment. The tephra layers are predominately unstratified with normal grain-size gradation, but also planar and cross stratified layers with overall reverse grading can occur, especially above erosive boundaries. Some ash layers are significantly more competent compared to their host sediment due to diagenetic processes and were tilted, bent and dissected during coring. Generally moderate, but partly extensive bioturbation has locally destroyed the primary sediment structures.

Juvenile particles of white to light gray ash beds are mainly (>90 vol%) composed of fresh, clear, colorless, glass shards varying from highly vesicular, pumiceous textures with commonly tubular and elongated bubbles to angular blocky, cusped, flat and y-shaped shards with very few vesicles (Figures 3 and 4). Grain sizes range from fine ash to coarse lapilli. The mineral assemblages comprise, in order of abundance, plagioclase, clino- and orthopyroxene, quartz, amphibole (mostly of hornblende composition), ilmenite and magnetite, as well as biotite and sanidine, but modal proportions vary among tephra. Generally, the crystals do not exceed 1 to 10 vol% in total.

Dark-gray mafic ash layers consist predominantly of dark brown glass shards. Most of these have blocky shapes and are moderately to poorly vesicular (Figure 3h). More mafic, dark gray to black tephra layers commonly have brownish glass shards with round to elliptical vesicles but tachylitic fragments are also observed. Some black ash layers also contain highly vesicular, tubular, brownish glass shards. The mineral assemblages of the dark tephra include plagioclase, pyroxene, Fe-Ti oxides and some olivine.

Glass-shard compositions of the Aegean marine tephra mostly range from andesitic to rhyolitic compositions with a few basaltic-andesitic samples (Figure 5a). Two glass-shard groups deviate significantly in having trachy-basaltic and trachyphonolitic compositions (Figure 5a). Apart from these two groups, all other samples straddle widely around the dividing line between between normal and high-K calc-alkaline compositions (Figure 5b).

### 6.2. Juvenile Glass Compositions of Proximal (Onshore) Tephra

We present the first published major and trace element glass compositions for Milos tephra. Moreover, for many other tephra we provide the first published trace element glass compositions. Figure 6 illustrates the compositional variabilities within and among the onshore tephra and eruptive centers. In many cases, tephra glass

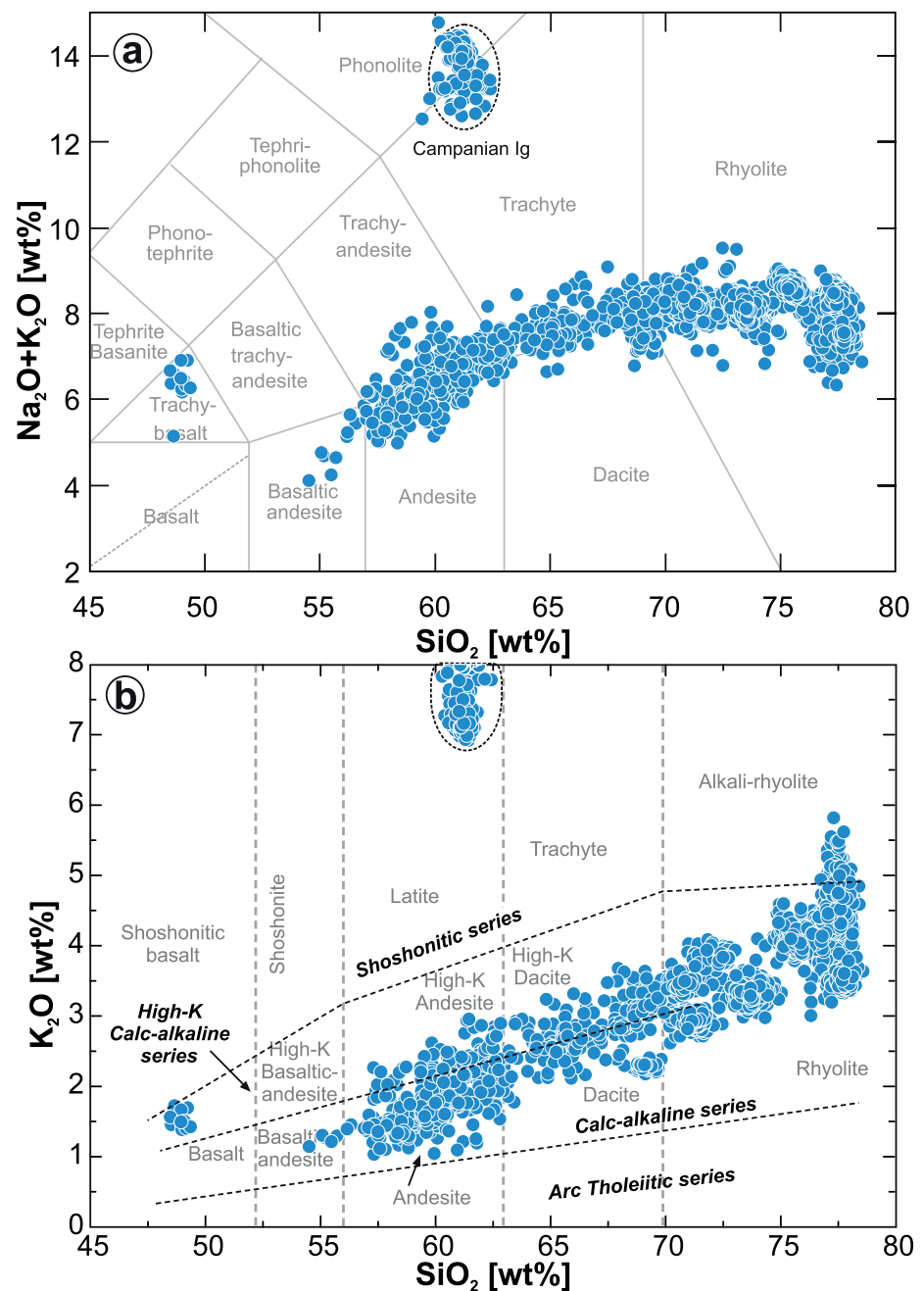


**Figure 5.** Glass-shard compositional ranges of marine tephras in POS513 cores (normalized to 100 wt% anhydrous compositions). (a) Total alkalis versus silica diagram showing the volcanic rock classification after Le Maitre et al. (2002). Most samples follow an andesite to rhyolite trend but note the separate trachybasaltic and trachyphonolitic groups. (b) Potassium versus silica diagram showing the classifications after Peccerillo and Taylor (1976).

compositions can be well discriminated by major element concentrations but in other cases there is significant overlap. Further distinctions can then be made on the basis of trace element ratios.

### 6.3. Correlation of Marine Ash-Layers With Their Volcanic Source

Figures 7 and 8 show a compilation of glass geochemical variation diagrams that are most useful for the purpose of correlation. All correlations are also compiled in Table 1. These correlations are supported by results from hierarchical cluster analyses (Figure 9) using 88 chemical elements and element ratios. Cluster analysis

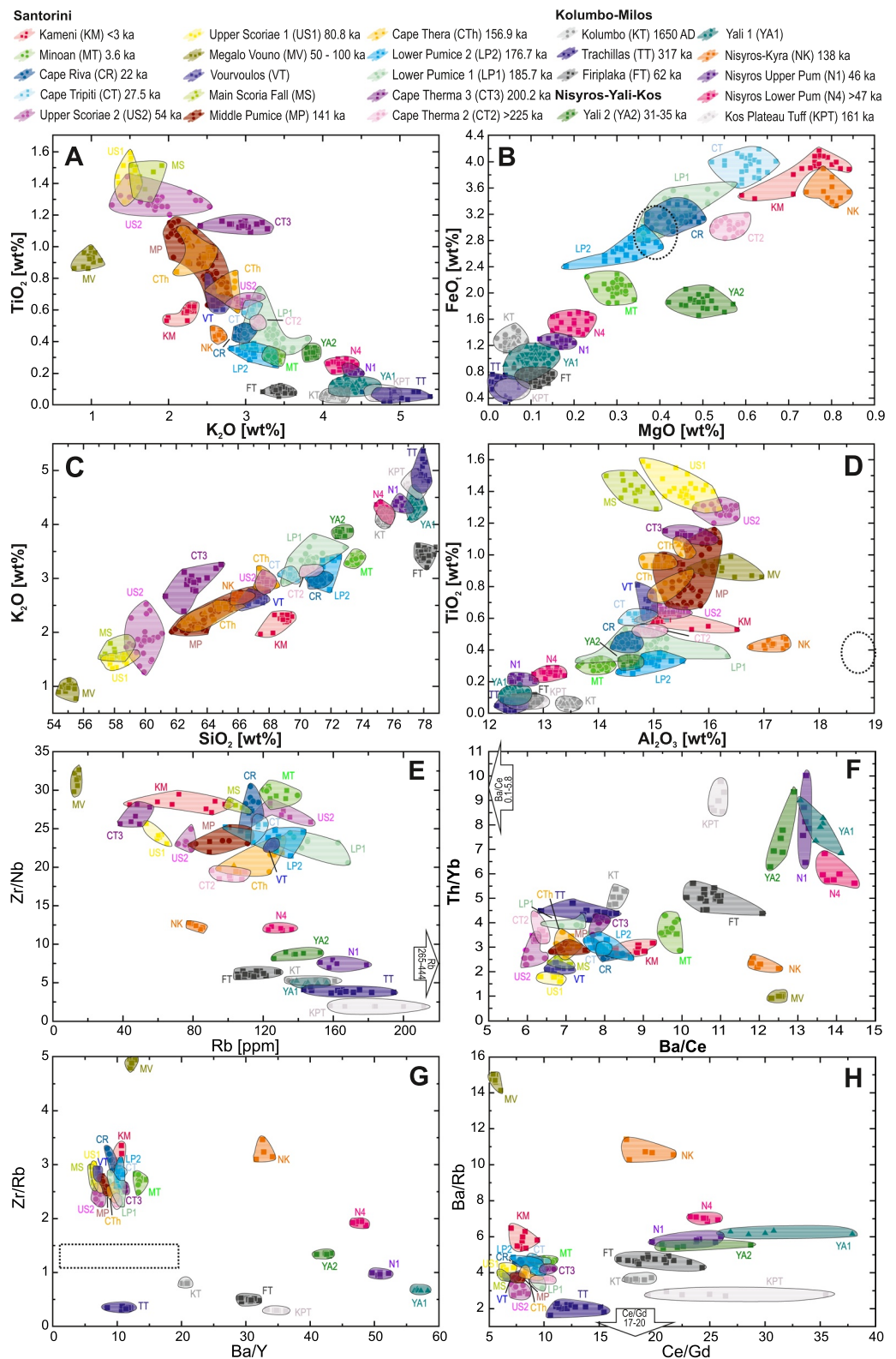


**Figure 6.** Matrix-glass compositional ranges of proximal onshore tephras (normalized to 100 wt% anhydrous compositions). Colored areas represent the correlation fields enclose the single measurements. See data in supplementary tables in Data Set S1.

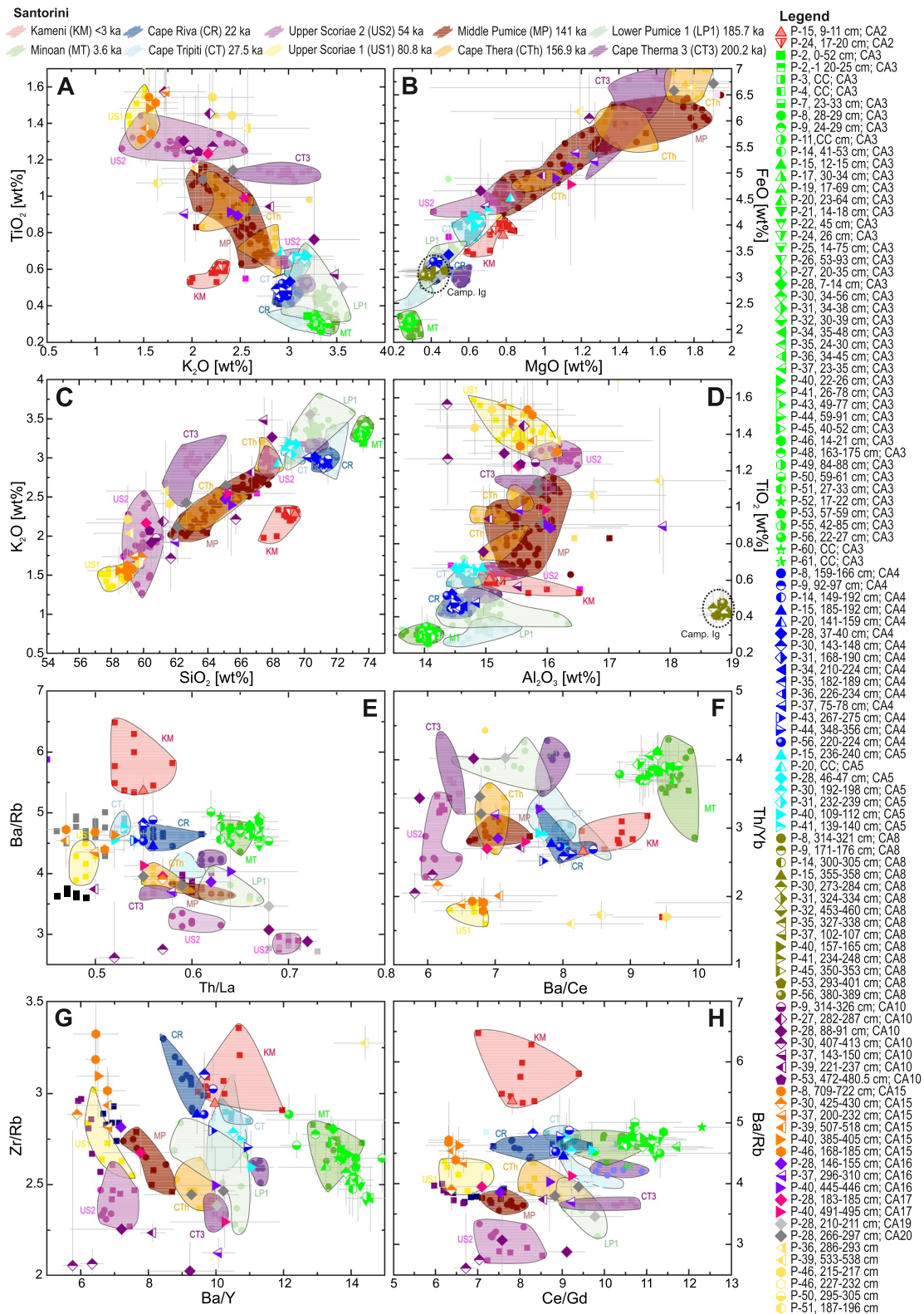


Figure 7.

successfully reproduces known stratigraphic relations of the tephra. The compositions of glass shards suggest that pods and sediment layers that contain dispersed ash commonly occur in the correct stratigraphic context, implying that redeposition of ash having occurred soon after or contemporaneous with the primary emplacement or that disturbance was by in-situ bioturbation.

In summary, we have been able to correlate 209 marine tephra layers to 19 Aegean tephra onshore as well as one tephra from the Campi Flegrei, Italy. Correlated marine tephra layers are labeled CA1 through CA20 in stratigraphic order from young to old. The remaining (11) uncorrelated ash horizons have compositions not represented in our database.

### 6.3.1. Milos Volcanic Complex

The pyroclastic sequences in unit 4 on Milos formed during at least three major eruptive events (e.g., Figure 2; Fytikas et al., 1986). From bottom to top, the succession of the past ~370 ka comprises the Trachilas tephra(s?) in the north, and the lower and upper Firiplaka tephra(s?) in the south (Campos Venuti & Rossi, 1996; Fytikas et al., 1986; Stewart & McPhie, 2006). Ages and distribution of the explosive and effusive eruption products beyond the island are not well constrained but new Ar/Ar ages for the younger pyroclastic sequence are  $317 \pm 4$  ka for the Trachilas complex and  $62 \pm 3$  to  $70 \pm 10$  ka and  $110 \pm 20$  ka, for the upper and lower Firiplaka tephra, respectively (Zhou et al., 2021). Furthermore, Campos Venuti and Rossi (1996) distinguished three members within the Firiplaka sequence comprising ~50 pyroclastic flow units in total.

Tephra layer CA7 occurs in cores POS513-7, -8, -9, -28, -32, -35, 3-9, -40, -41, -46, -52, -53, -54, and -56 as a distinct bed or pod layers with thicknesses from 1 to 30 cm (Figures 7 and 8; Tables 1 and S3 in Data Set S1). Tephra layer CA7 correlates geochemically with the youngest Firiplaka tephra samples sampled by Nomikou and colleagues in 2018 at the tuff ring (FT, Figures 7 and 8; Tables 1 and S1 in Data Set S1). Both major and trace elements as well as the statistical clustering provide unambiguous links between the onshore and marine tephra samples. The  $\text{Na}_2\text{O}/\text{K}_2\text{O}$  ratios, as pointed out by Fytikas et al. (1986), facilitate the distinction between Trachilas ( $\text{Na}_2\text{O}/\text{K}_2\text{O} < 1$ ) and Firiplaka ( $\text{Na}_2\text{O}/\text{K}_2\text{O} > 1$ ) tephra; the marine CA7 tephra has  $\text{Na}_2\text{O}/\text{K}_2\text{O} > 1$ , matching the Firiplaka unit (Table S3 in Data Set S1).

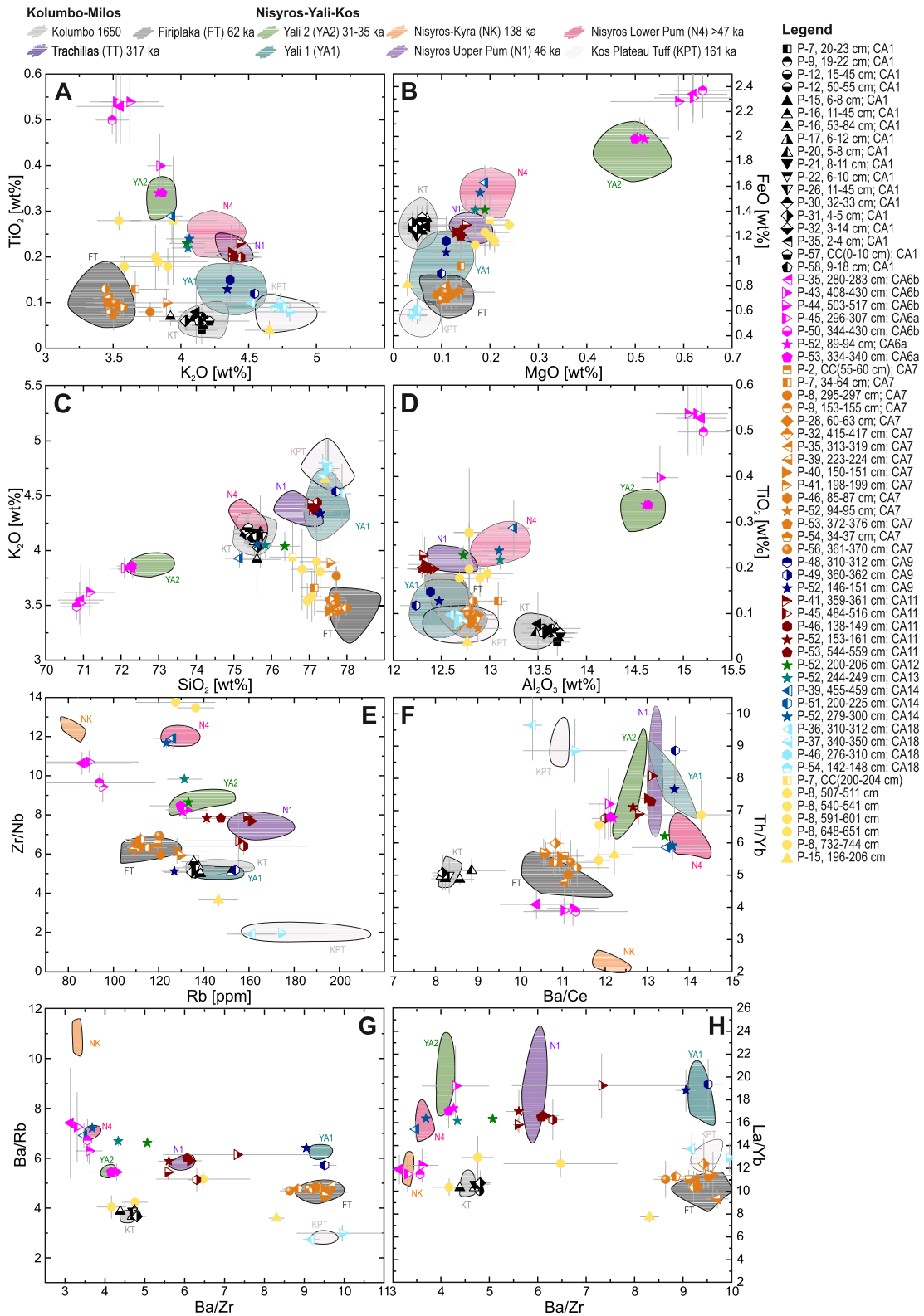
Phenocrysts in the crystal-poor (<10%) pumices of the onshore Firiplaka deposits comprise abundant plagioclase, sanidine, quartz, and lesser biotite and amphibole (Fytikas et al., 1986), which is consistent with the mineral assemblage and the order of abundance we found in the marine ashes (<5% crystals).

The major element glass composition of a 0.3 cm thick marine ash layer 133.1–133.4 cm bsf (below sea floor) in core TR172-26 (Figure 1b) described by Hardiman (1999) is a possible match with Firiplaka tephra. With this and our core POS513-54, the Firiplaka tephra extends at least 200 km to the southeast from Milos.

### 6.3.2. Santorini

The pyroclastic sequence emplaced on Santorini during the past ~360 kyrs contains 13 tephra from major, dominantly silicic and intermediate eruptions (Figure 2), including at least four caldera-forming events (Lower Pumice 2, Upper Scoriae 1, Cape Riva, Minoan; Druitt et al., 1989, 1999; Druitt & Francaviglia, 1992). All Santorini tephra have more or less similar mineral assemblages and minor to moderate crystal contents (5%–20%) consisting of dominant plagioclase and subordinate clino- and orthopyroxene, Fe-Ti oxides and  $\pm$  pyrrhotite and apatite; some dacitic and rhyodacitic tephra also have rare amphibole whereas andesites also may include olivine (Druitt et al., 1999; Vespa et al., 2006). Numerous deposits from smaller, inter-plinian eruptions are intercalated between the major tephra (Druitt et al., 2016), some of which are postulated to be present in marine cores by Wulf et al. (2020). Since trace element glass compositions of inter-plinian tephra are not available, we tested possible correlations of marine tephra with the inter-plinian units by comparing major-element glass compositions

**Figure 7.** Glass-shard compositions of marine ash layers (normalized to 100 wt% anhydrous compositions) recovered from the western part of our research area around the CSK volcanic complex, compared with glass-composition fields for Santorini onshore tephra shown in Figure 6. Marine data symbols are averages of all analyses for each ash layer and the attached gray bars indicate the standard deviation around the mean. The analytical data are given in the supplementary tables in Data Set S1. Marine ash samples identified by symbols are listed at right by core number, depth below seafloor, and correlated tephra layer CAx. The color coding groups ash layers that belong to the same tephra layer CAx. The legend at top identifies colored composition fields of the onshore tephra.



with their data (see Figure S1) but mostly found no unambiguous correlation. One exception is marine tephra layer CA5 which would fit the major element composition of inter-plinian tephra associated with the Cape Tripiti tephra (Figure S1; Wulf et al., 2020). However, as we will show below, we prefer to correlate CA5 with the Cape Tripiti tephra itself because of the good trace element fits. It is possible, however, that Cape Tripiti tephra and associated inter-plinian tephra are indistinguishable, also in trace element compositions.

Starting with the oldest Santorini tephra in the marine sequence, the 30-cm-thick ash layer CA20 in core POS 513–28 (266–297 cm bsf) has a glass-chemical composition matching that of Cape Thera, Cape Therma 3 and Middle Pumice, which are all very similar (Figures 7 and 9, Tables 1 and S3 in Data Set S1). However, there is a general decrease in silica from bottom to top of the inversely graded marine ash layer that may reflect the compositional zonation observed in the Cape Therma 3 tephra on land, where a basal greyish-orange pumice fall is overlain by gray to pink to black andesitic scoria flow deposits (Druitt et al., 1999; Wulf et al., 2020). Additionally, CA20 occurs stratigraphically below Lower Pumice 1 (186 ka) in the same core, excluding a possible correlation with Cape Thera and Middle Pumice which are both younger than Lower Pumice 1. We therefore favor a correlation of CA20 with the  $200.2 \pm 0.9$  ka old (Wulf et al., 2020) Cape Therma 3 tephra. Wulf et al. (2020) also geochemically correlated a 2.5 cm thick ash layer at 639.5 cm bsf in RV Meteor M40/4 core KL51, which also has dacitic to andesitic glass compositions, to the Cape Therma 3 tephra.

Tephra layer CA19 occurs in core POS 513–28 (210–211 cm bsf) and matches the glass composition of the  $185.7 \pm 0.7$  ka old onshore Lower Pumice 1 (LP1, Figure 7; Tables 1 and S3 in Data Set S1), a prominent white pumice fall layer underlain and overlain by pyroclastic flow deposits with white to gray pumice clasts, abundant lithic clasts, and obsidian clasts (Druitt et al., 1999; Simmons et al., 2016; Wulf et al., 2020). Cluster analysis confirms this correlation very well (Figure 9). The marine ash layer V3 in the southern to southwestern Mediterranean Sea (Keller et al., 1978) and in core KB26 (156–158 cm) southeast of Crete (Vinci, 1985), also occurs in core M40/4-KL51 (594 cm bsf, also southeast of Crete) where it has been correlated with LP1 by Wulf et al. (2020).

Lower Pumice 2 tephra (LP2) consists of a ~20-m-thick, coarse grained, normally graded fall deposit of white pumice clasts in the western cliffs of Thira, overlain by several meter-thick pyroclastic flow deposits (Druitt et al., 1999; Keller et al., 2014; Simmons et al., 2017). We did not find equivalents of the  $176.7 \pm 0.6$  ka old (Wulf et al., 2020) LP2 tephra in our cores, but Wulf et al. (2020) correlated a layer in core M40/4-KL51 (529 cm bsf) with LP2 and they reported that this layer has previously been correlated by Hieke et al. (1999) to Keller's V-1 tephra (Keller et al., 1978).

Two-to 4-cm-thick tephra layer CA17 is found in cores POS 513–28 (183–185 cm bsf), and –40 (491–495 cm). Its glass composition falls in the overall cluster of Middle Pumice, Cape Therma 3 and Cape Thera (CTh, Figures 7 and 8; Tables 1 and S1 in Data Set S1). However, there are additional observations that lead us to favor a correlation with the  $156.9 \pm 2.3$  ka Cape Thera tephra. First, dark marine tephra layer CA17 contains transparent to brownish glass shards that have a broad range in compositions (e.g., 55 to 70 wt% SiO<sub>2</sub>, mean 63 wt% SiO<sub>2</sub>) which reflects the compositional heterogeneity of the trachy-andesitic to trachy-dacitic compositions found in the pumice fall and scoria flow deposits on land (Druitt et al., 1999; Wulf et al., 2020). Second, CA17 assumes a stratigraphic position in the cores between ash layers that correlate with Lower Pumice 1 and Middle Pumice or Upper Scoriae 1, respectively. CTh has also been assigned to ash layers in cores KL51 (498.5 cm bsf) and LC21 (1,077–1,119 cm bsf) by Wulf et al. (2020). Applying our major element correlation fields to the glass data of Hardiman (1999) suggests also correlation with an ash layer in core TR172/27 (305–307 cm bsf).

Tephra layer CA16 is found as dispersed ash in core POS 513–28 (146–155 cm bsf) and as a distinct layer of 1–14 cm thickness (Figure 3f) in cores POS 513–40 (445–446 cm bsf) and POS 513–37 (296–310 cm bsf). It correlates compositionally with the Middle Pumice (MP, Figure 7; Tables 1 and S3 in Data Set S1) and all three marine-bed compositions are confined to the same cluster branch as the onshore sample from the upper part of the

---

**Figure 8.** Glass-shard compositions of marine ash layers (normalized to 100 wt% anhydrous compositions) recovered from the eastern part of our research area around the Kos-Yali-Nisyros (KYN) volcanic complex, Kolumbo Volcano, and Milos volcanic complex, compared with glass-composition fields onshore Milos, KYN, and for Kolumbo tephra shown on Figure 6. Marine data symbols are averages of all analyses for each ash layer and the attached gray bars indicate the standard deviation around the mean. The analytical data are given in the supplementary tables in Data Set S1. Marine ash samples identified by symbols are listed at right by core number, depth below seafloor, and correlated tephra layer CAx. The color coding groups ash layers that belong to the same tephra layer CAx. The legend at top identifies colored composition fields of the onshore/proximal tephra.

---

**Table 1**  
Summary of Marine Tephra Correlations Within the Christiana-Santorini-Milos Region and to the Proximal Tephra of the Aegean Volcanic Arc

Correlation	Acronym	Volcanic complex	Age [ka] from literature	Correlation #	Occurrence in POSS13 cores	Representative elements, concentrations and ratios for Aegean arc correlations					
						K <sub>2</sub> O	SiO <sub>2</sub>	CaO	Ba/Ce	Zr/Nb	Ce/Gd
Kolumbo	<b>KT</b>	Kolumbo volcano	<b>1650ADh</b>	<b>CA1</b>	7_8-10; 9_14-15; 12_15-55; 15/21_2-6; 16_11-84; 17_3-5-8.5; 20_5-8; 14/22_6-10; 26_19-44; 30_16-18; 31_4-5; 32_3-14; 35_2-4; 57_CC; 58_9-18	3.9-4.2	75.3-75.8	0.7-0.8	8.1-8.9	5.0-5.6	17.5-19.7
Kameni	<b>KM</b>	Kameni island		<b>CA2</b>	15_9-12; 24_16-19	2.2-2.3	69.1-69.4	2.7-2.8	8.2-8.3	25.5-25.8	7.6-7.9
Minoan	<b>MT</b>	Santorioni	<b>3.6 BCD</b>	<b>CA3</b>	2_0-52; 2_1_20-25; 3_CC; 4_CC; 7_23-25; 8_28-29; 9_25-29; 11_CC; 12_50-51; 14/22_41-53; 15_16-19; 17_32-36; 19_17-69; 20_23-64; 21_14-18; 24/25_14-75; 26_55-93; 27_18-35; 28_7-14; 30_33-56; 31_34-38; 32_30-39; 34_35-48; 35_24-30; 36_34-45; 37_23-35; 40_22-26; 41_26-78; 43_49-77; 44_59-91; 45_40-51; 46_14-20; 48_163-175; 49_84-88; 50_59-60.5; 51_27-33; 52_16-21; 53_53-69; 55_42-85; 56_22-27; 60_CC; 61_CC	3.2-3.5	73.0-73.9	1.4-1.7	8.8-9.7	26.1-31.2	9.8-12.3
Cape Riva	<b>CR</b>	Santorioni	<b>22.0 ± 0.3D</b>	<b>CA4</b>	8_159-166; 9_92-97; 14/22_149-192; 15_185-192; 20_141-159; 28_37-40; 30_143-148; 31_168-190; 34_210-224; 35_182-189; 36_226-234; 37_75-77.5; 43_267-275; 44_348-356; 56_220-224	2.6-3.0	70.2-71.5	1.8-2.3	7.7-8.5	24.1-29.7	8.3-9.2
Cape Tripiti	<b>CT</b>	Santorioni	<b>27.5 ± 0.7D</b>	<b>CA5</b>	15_236-240; 20_CC; 28_46-47; 30_192-198; 31_232-239; 40_109-112; 41_139-140	2.9-3.2	68.4-69.4	2.3-2.7	7.6-8.0	22.7-25.2	8.4-9.7
Yali 2a	<b>YA2</b>	Yali	<b>31-33 ka</b>	<b>CA6a</b>	45_297-307; 52_73-92; 53_334-340	3.8-3.9	72.1-72.3	2.0-2.1	12.1-12.2	8.2-8.5	21.7-23.9
Firiplaka	<b>FT</b>	Milos		<b>CA7</b>	35_280-283; 43_408-430; 44_503-517; 50_363-430(CC)	3.5-3.6	70.8-71.2	2.2-2.4	10.4-11.3	9.4-10.7	15.6-18.0
Campian Ignimbrite	<b>CP</b>	Campi Flegri	<b>39.85 ± 0.14D</b>	<b>CA8</b>	2_1_CC; 7_42-64; 8_295-297; 9_153-155; 28_60-63; 32_415-417; 35_313-319; 39_221-221; 40_150-151; 41_198-199; 46_84-85; 52_95-95.5; 53_372-376; 54_34-37; 56_361-370	3.4-3.9	77.1-78.0	0.8-1.1	10.6-11.4	5.9-7.0	17.6-21.0
Yali 1	<b>YA1</b>	Yali		<b>CA9</b>	8_316-321; 9_172-176; 14_300-305; 15_355-358; 30_273-284; 31_324-334; 32_453-460; 35_327-338; 37_102-107; 40_157-165; 41_235-248; 45_350-353; 53_393-400.5; 56_385-389	6.7-8.0	61.1-67.3	1.9-2.1	0.07-0.12	4.7-5.9	20.8-23.0
					48_310-315; 49_362(CC); 52_147-151.5	4.3-4.5	77.1-77.7	0.6-0.8	13.3-13.7	5.1-5.2	27.2-30.2

continued

Correlation	Acronym	Volcanic complex	Age [ka] from literature	Correlation #	Occurrence in POSS13 cores	Representative elements, concentrations and ratios for Aegae arc correlations					
						K <sub>2</sub> O	SiO <sub>2</sub>	CaO	Ba/Ce	Zr/Nb	Ce/Gd
Upper Scoria 2	US2	Santorini	<b>54 ± 3D</b>	CA10	9_314-326; 27_CC; 28_88-91; 30_407-412; 37_143-150; 39_232-239; 53_482-487	1.5-3.4	58.3-68.0	2.7-6.3	5.8-7.4	21.0-27.2	6.4-9.1
Nisyros 1 (Upper Nisyros Pumice)	N1	Nisyros	29 - 70 ka	CA11	41_359-361; 45_484.5-516; 46_139-146; 51_200-225; 52_156-160; 53_535-559(CC)	4.3-4.6	77.0-77.3	0.8-0.9	12.0-13.3	4.5-7.9	23.2-29.4
Nisyros 2	N2	Nisyros		CA12	52_202-206	3.9-4.2	76.0-76.8	0.9-1.1	13.3-13.5	8.5-8.9	22.6-29.4
Nisyros 3	N3	Nisyros		CA13	52_246-249	3.9-4.2	75.7-76.0	0.8-0.9	13.4-13.9	9.7-10.0	22.7-26.6
Nisyros 4 (Lower Nisyros Pumice)	N4	Nisyros	>70 ka	CA14	39_450-458; 52_297-300(CC)	3.9-4.2	75.2-76.4	0.9-1.0	13.4-13.6	9.5-11.9	22.9-24.7
Upper Scoria 1	US1	Santorini	<b>80.8 ± 2.9D</b>	CA15	8_709-722; 30_427-440; 37_206-232; 39_508-514; 40_385-403; 46_182-187	1.5-1.7	58.2-59.9	5.7-6.5	6.2-7.1	24.0-26.3	6.3-6.7
Middle Pumice	MP	Santorini	<b>141.0 ± 2.6D</b>	CA16	28_146-155; 37_296-310; 40_445-446	1.9-2.5	62.0-65.4	3.6-5.2	7.0-7.7	19.5-24.8	7.5-9.2
Cape Thera	CTh	Santorini	<b>156.9 ± 2.3D</b>	CA17	28_183-185; 40_491-495	2.2-2.5	60.1-65.2	4.0-6.0	6.9-7.4	19.2-21.9	7.1-9.2
Kos Plateau Tuff	KPT	Kos	<b>161.3D</b>	CA18	36_CC; 37_342-348; 46_300-310; 54_142-148	4.5-4.8	77.4-77.9	0.6-0.7	10.3-11.3	1.9-2.4	20.3-24.6
Lower Pumice 2	LP2	Santorini	<b>176.7 ± 0.6D</b>								
Lower Pumice 1	LP1	Santorini	<b>185.7 ± 0.7D</b>	CA19	28_210-211	3.3-3.6	66.4-68.6	1.6-2.1	7.0-7.4	20.5-21.9	9.1-10.5
Cape Thera 3	CT3	Santorini	<b>200.2 ± 0.9D</b>	CA20	28_266-297	2.1-2.6	62.1-65.1	3.6-5.1	6.7-6.8	20.7-20.9	8.8-9.4

Note: D: radiometric and/or sedimentation rate ages associated with sapropels from Druitt et al., 1999, Bronk Ramsey et al., 2015, data from Keller cited in Vespa et al., 2006 and Gertisser et al., 2009, Giaccio et al., 2017, Satow et al., 2015, Wulf et al., 2020 h: historic ages. This only important in the age column where bold/italic are radiometric ages and only italic ones are estimates.

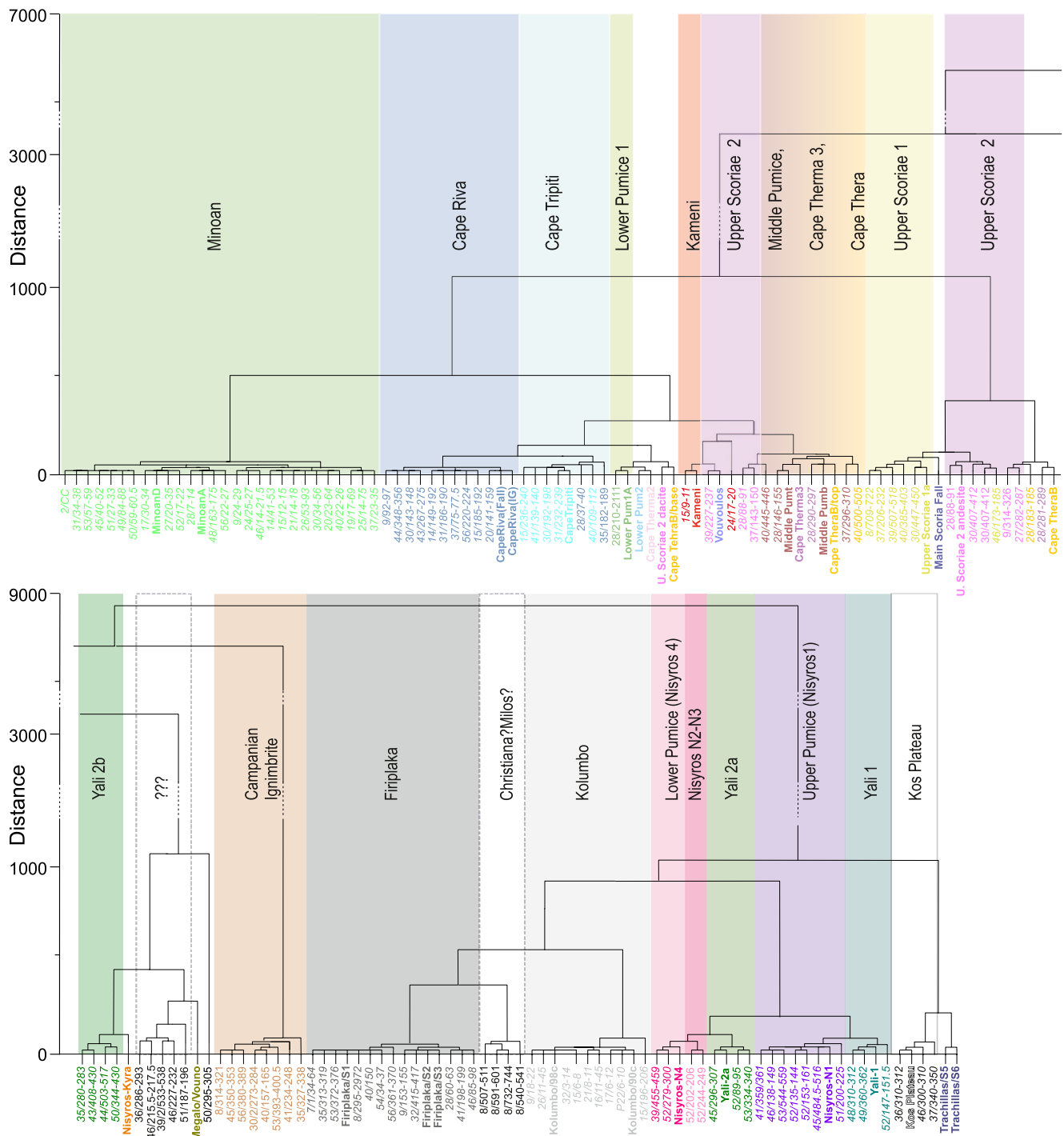


**Figure 9.** Dendrograms of hierarchical cluster analysis (squared Euclidean distance, Ward method) using 10 principal components obtained by principal component analysis of 88 elements and element ratios. The 147 tested samples include average compositions of 113 marine tephra and 34 onshore tephra. With rare exceptions the correlations observed in Figures 7 and 8 are verified by the respective cluster grouping. Only the glass compositions of Middle Pumice, Cape Therna 3 and Cape Therna tephra are too similar to be discriminated. Note that distance scales are interrupted for clarity.

MP fall deposit (Figure 9). MP was additionally found by Wulf et al. (2020) in core KL51, 452.5–455 cm bsf, by Federman and Carey (1980) in TR172/19 and 27, and by Vinci (1985) in core KB28 327–330 cm bsf.

Tephra layer CA15 occurs as distinct beds in cores POS 513–8 (709–722 cm bsf), –30 (412–447 cm bsf), –37 (206–232 cm bsf), –39 (507–518 cm bsf), –40 (385–405 cm bsf), and –46 (173–185 cm bsf).

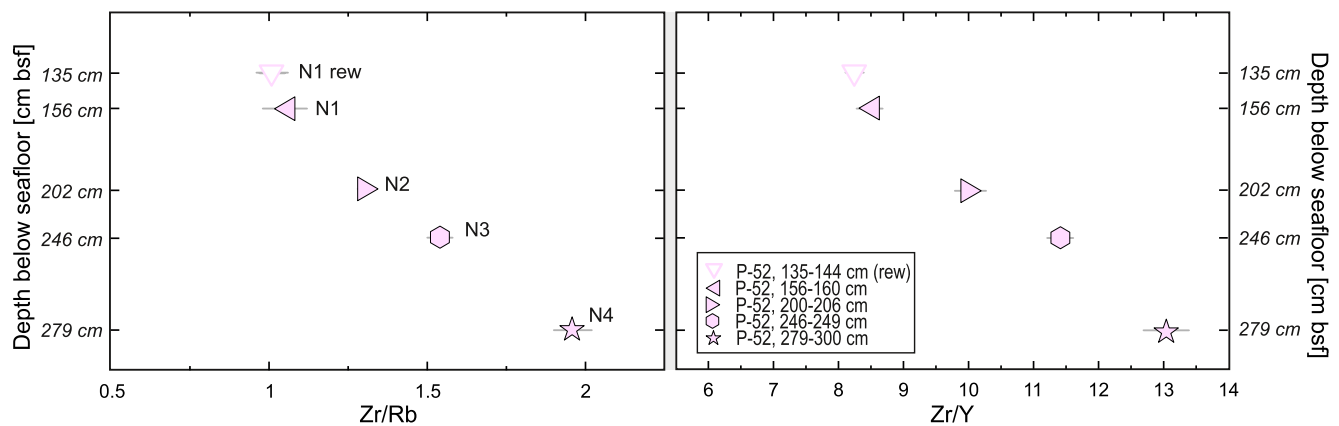


**Figure 10.** Variation of selected trace element ratios of the glass shard compositions of the Nisyros N1 to N4 ash layers with depth below seafloor in core POS513-52. The four ash layers have clearly distinct compositions and hence represent separate eruptions. They also form a systematic evolutionary trend which attests to their eruption from an evolving magma reservoir. Reworked (rew) N1 ash ~10 cm above the primary N1 layer shares the same glass shard composition. Symbols are averages of all analyses made for each tephra with the range of individual measurement compositions given by the gray bars.

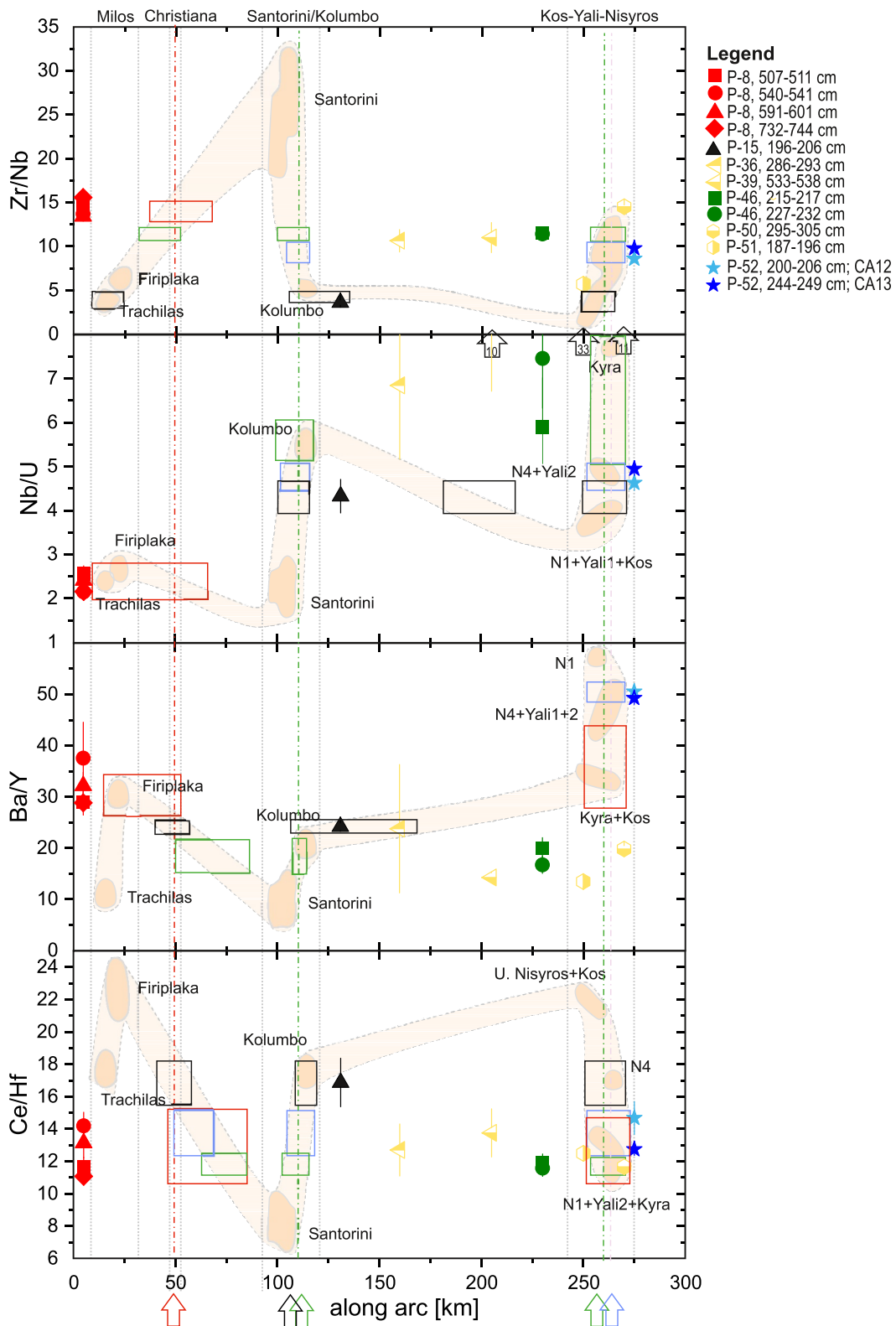
The 3- to 32-cm-thick tephra layer (Figures 3e and 3h) correlates with the Upper Scoriae 1 deposit onshore (US1, Figure 7; Tables 1 and S3 in Data Set S1) that is described as a major dark scoria fall overlain by a series of massive pyroclastic flow deposits containing coarse-grained spatter agglomerates (Druitt et al., 1999). Tephra layer CA15 is mainly composed of brown glass shards with characteristic andesitic composition that falls into one cluster subgroup together with the onshore sample Upper Scoriae 1a (Figure 9). Moreover, the marine tephra also contains a few glass shards of trachy-andesitic composition as well as some rare olivine crystals both of which are also observed in its onshore US1 counterpart (Andújar et al., 2016; Wulf et al., 2020). US1 was also recognized in other cores by Wulf et al. (2020) who also assigned layer X-1 from Keller et al. (1978) and ash beds in numerous other cores of Hardiman (1999) and Aksu et al. (2008) to US1, following the suggestion of Hieke et al. (1999) and Schwarz (2000). Our revisiting of the given literature data confirms these correlations.

Another prominent black marine tephra layer, CA10, can be correlated with Upper Scoriae 2 (US2, Figure 7; Tables 1 and S3 in Data Set S1). It is 7–12 cm thick in one core west (POS 513–9, 314–326 cm bsf) and six cores east (POS 513–27, –28, –30, –37, –39, –53) of Santorini. Marine and onshore Upper Scoriae 2b samples together fall into one confined cluster subgroup (Figure 9). Similar to Upper Scoriae 1, supporting arguments for this correlation are the rare occurrence of olivine and the range of glass compositions from andesite to dacite in the marine ash, which reflect the andesitic bulk-rock composition of onshore US2, being dominated by spatter agglomerates (Druitt et al., 1999).

Tephra layer CA5 occurs in cores POS 513–15, –20, –28, –30, –31, –40, and –41 as a 1- to 7-cm-thick distinct ash bed or ash pod layer. It correlates with the up to 1-m-thick rhyodacitic onshore deposits from the  $27.5 \pm 1.2$  ka old Cape Tripiti eruption (CT, Fabbro et al., 2013; Satow et al., 2015) on the basis of major and trace element glass compositions (Figure 7; Tables 1 and S3 in Data Set S1) and is distinct from other large Santorini tephtras. Apart from one sample, the glass compositions of Cape Tripiti and Cape Riva tephtras are very well discriminated in two related branches of the cluster analysis, supporting the correlation (Figure 9). As discussed above, minor inter-plinian pyroclastic fall layers at this stratigraphic level have the same major-element glass compositions as Cape Tripiti tephra and their contribution to CA5 cannot presently be excluded (see Figure S1).

CA5 is also correlative to 1- to 5-cm-thick ash layers in other cores of the region (LC21, V10-58, TR172-26,27, MC10, 12) at the same stratigraphic position when comparing our onshore database to their major element data for single layers (Hardiman, 1999; Satow et al., 2015, 2020; Vinci, 1985), as well as considering the stratigraphic position between tephra layers Y-2 (Cape Riva) and Y-5 (Campanian Ignimbrite) as shown for core V10-58 (Y-4; Keller et al., 1978). This correlation was proposed by Wulf et al. (2020) following Fabbro et al. (2013).

One of the tephtras most frequently found in our cores is layer CA4, which occurs as ash layers occasionally showing both fall and flow facies (Figure 3b). CA4 is present as 3- to 43-cm-thick ash layers in cores POS 513–8, –9, –14, –15, –20, –28, –30, –31, –34, –35, –36, –37, –43, –44, and –56 between 20 and 130 km



from Santorini. The rhyolitic glass shards facilitate the correlation with the  $22.0 \pm 0.3$  ka old (Bronk Ramsey et al., 2015), rhyodacitic, Cape Riva Tephra (CR, Figure 7; Tables 1 and S3 in Data Set S1) that is associated with the third caldera-forming eruption of Santorini. This eruption emplaced a thick pumice fall deposit followed by a thick ignimbrite (Druitt et al., 1999). Fragments of andesitic scoria enclaves that are found in the onshore samples are very rarely found in the marine ash layers. The marine samples share a sub-cluster with the onshore Cape Riva samples (Figure 9); one sample, POS 513–28, 37–40 cm shares the Cape Tripiti sub-cluster but can be distinguished within this core from underlying Cape Tripiti due to its major element composition (Figure 7). On a regional scale, CA4 correlates with the widespread Y2 layer of Keller et al. (1978) and is also recognized in numerous other cores around the Aegean Sea, indicated by Federman and Carey (1980), Vinci (1985), Aksu et al. (2008), Margari et al. (2007), and Wulf et al. (2002, 2020).

The most frequently occurring marine tephra in the entire region is tephra layer CA3 (in all cores except POS 513–16, 39 and 54), which correlates with the 3.6 ka old Minoan eruption, the latest caldera-forming event on Santorini (Druitt et al., 1999). The correlation is supported by the fairly unique glass compositions (MT, Figure 7; Tables 1 and S3 in Data Set S1), by the well discriminating cluster analysis (Figure 9) and by the shallow position mostly <50 cm below the sea floor. CA3 consists of highly vesicular pumiceous particles (Figures 3g and 3l) and has thicknesses from 1 to 61 cm; both fall and flow facies can be observed (Figure 3a). Marine ash of the Minoan eruption (Z2 tephra after Keller et al., 1978) occurs in multiple cores all over the Mediterranean Sea and adjoining onshore regions (e.g., Aksu et al., 2008; Federman & Carey, 1980; Hardiman, 1999; Margari et al., 2007; Satow et al., 2015; Vinci, 1985; Wulf et al., 2020).

The tephra layer CA2 occurs in two cores (POS 513–15, 9–11 cm bsf; POS 513–24, 17–20 cm bsf) within 60 km of Santorini. The glass composition is similar to that of deposits from the larger explosive eruptions of Kameni (KM, Figures 7 and 9; Tables 1 and S3 in Data Set S1) suggesting an origin from that volcano although not necessarily from the specific eruption of the sampled Kameni tephra.

### 6.3.3. Kolumbo Submarine Volcano

The youngest tephra layer identified in our cores (CA1) has a unique major and trace element glass composition and, in contrast to Santorini tephtras, contains biotite (c.f. Cantner et al., 2014; Fuller et al., 2018). CA1 can be unambiguously correlated with the 1650 AD eruption of Kolumbo submarine volcano using the correlation diagrams and the cluster analysis (KT, Figures 8j and 9; Tables 1 and S3 in Data Set S1). Cores containing CA1 occur from 10 to 140 km distance from Kolumbo Volcano (POS 513–7, –9, –12, –14, –15, –16, –17, –20, –21, –26, –30, –31, –32, –35, –57, and –58). The CA1 tephra occurs either as a discrete thin ash layer or ash pod layer (1–4 cm thick) or as complex multi-layered thick tephra sequences (6–73 cm; Figure 3a). A mixture of blocky and pumiceous glass shards (Figures 3k, 3m–3o) is characteristic of the Kolumbo marine ash.

### 6.3.4. Kos

We have not found tephra CA18 as a distinct primary ash layer in our cores but it occurs as dispersed ash (about 50 vol%) in a ~10-cm- and 6-cm-thick sediment layer (POS 513–37, 340–350 cm bsf, POS 513–54, 142–148 cm bsf, respectively) and in the deformed sample recovered in two core catchers (POS 513–46, 300–310 cm bsf and POS 513–36, 310–312 cm bsf). These core positions lie about 80 km southwest of the KYN volcanic complex, and the glass compositions correlate well with the Kos Plateau Tuff (KPT, Figures 8 and 9; Tables 1 and S3 in Data Set S1) in agreement with the stratigraphic position beneath all other KYN tephtras in the cores (Figure 2). Marine ash beds of the Kos Plateau Tuff have also been reported by Federman and Carey (1980), Vinci (1985), Hardiman (1999), Margari et al. (2007), Satow et al. (2015), and Wulf et al. (2020) in the Aegean Sea but also in the Black Sea by Wegwerth et al. (2019).

**Figure 11.** Comparison of average glass compositions of 13 uncorrelated ash beds with Zr/Nb, Nb/U, Ba/Y, and Ce/Hf variations along the Aegean Volcanic Arc (W to E) as discussed in the text. Gray dashed bars represent the geographical position of the volcanic centers along the arc. Note that we do not have glass compositions for Christiana. Along-arc variations are based on our own glass compositions measured in this work. The distance along the arc is measured from Antimilos eastward. Positions of tephtras along the *x*-axis are approximate locations of the cores in which they were found. Rectangles and associated arrows (colors are adapted from the respective marine ashes) at the *x*-axis represent the resulting best-fit location for the source areas of the unknown tephtras based on their compositions.

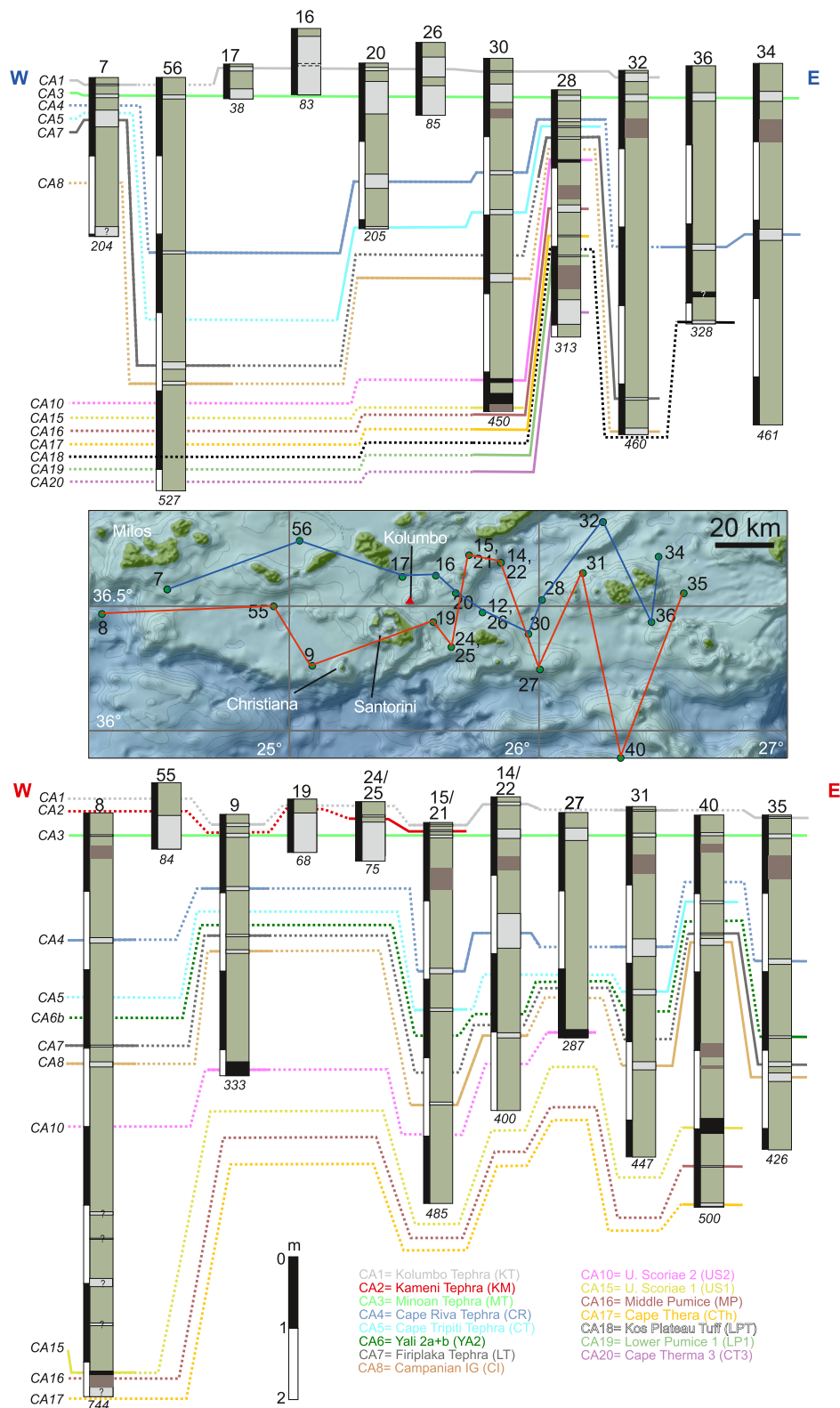


Figure 12.

### 6.3.5. Yali

We found the Yali 1 pumice breccia (Figure 2) glass composition in the 2- to 4-cm-thick tephra layer CA9 in three proximal cores (POS 513–48, –49, and –52) east of Yali and Nisyros (Y1, Figure 8; Tables 1 and S3 in Data Set S1). We found two tephra layers, CA6a and CA6b, that are bracketed by CA8 (Campanian Ignimbrite) and CA7 (Firiplaka Tephra) below and CA4 (Cape Riva Tephra) and CA5 (Cape Tripiti Tephra) above, where CA6a occurs in cores POS 513–45, –52, and –53 south of Yali and CA6b in cores POS 513–35, –43, –44, and –50 west of Yali. The glass composition of CA6a matches that of Yali-2 fall deposits on land (Figures 2 and 8; Tables 1 and S3 in Data Set S1) but the CA6b glass shards are slightly less evolved. In part 2 we will justify their interpretation as two contemporaneous, laterally separated facies produced by the Yali-2 eruption.

CA6a is also correlative with 1- to 9-cm-thick tephra layers in other cores of the region (LC21, TR172-18, –19, –21, –22, –24, –25, KB33) at the same stratigraphic position (Aksu et al., 2008; Hardiman, 1999; Satow et al., 2015; Vinci, 1985). Aksu et al. (2008) also described two consecutively emplaced tephra layers of related compositions between 351 and 360 cm bsf in core MAR03-24 that both match the compositions of our marine tephra layers CA6a and b.

### 6.3.6. Nisyros

The stratigraphy of Nisyros includes two major plinian tephra layers, the Upper and Lower Pumice deposits (Figure 2b; Volentik et al., 2002). However, core POS 513–52, 11 km from Nisyros, indicates that the (sub-)plinian history of this volcano may be more complex because there are four primary ash layers at 153–161, 202–206, 244–249, and 279–300 cm bsf (CA11 to CA14), which we call Nisyros1 to Nisyros4 (N1 to N4, Figure 4a), respectively. Layer N4 in core POS 513–52 forms part of the correlated tephra layer CA14 which shares the glass composition of the Lower Pumice (Figure 8; Tables 1 and S3 in Data Set S1) and thus lies in the same cluster subgroup (Figure 9). Layer N1 and tephra layer CA11, found in six other cores (POS 513–41, –45, –46, –51, –52, and –53), match the glass composition of the Upper Pumice (Figures 8 and 9; Tables 1 and S3 in Data Set S1). All Nisyros ash beds contain highly vesicular glass shards (Figures 4c and 4f) although some poorly vesicular shards also occur (Figure 4e).

The two fine-lapilli pumice layers N2 and N3 in core POS 513–52 (Figure 4a) each have unique glass compositions constraining their origin from separate eruptions (Figure 10). Their trace element characteristics favor an origin from Nisyros (Figure 11). Moreover, the glass compositions of N2 and N3 form a systematic trend with those of N1 and N4 (Figure 10) which suggests eruption of all four tephra layers from the same evolving magma reservoir. Deposits equivalent to the marine N2 and N3 tephra layers have not yet been found on land between the Lower and Upper Pumice deposits.

The Upper Pumice (N1) has also been found as 1–13 cm thick ash beds in other marine and lacustrine cores of the region (ML01, MAR03-49, –3, –27, –28, MC27, Theopetra cave) correlated by Vinci (1985), Margari et al. (2007), Aksu et al. (2008), Tomlinson et al. (2012) and Karkanis et al. (2015).

### 6.3.7. The Campanian Ignimbrite Ash Layers

The distinctive trachy-phonolitic composition (Figure 5), and characteristic trace element concentrations (e.g., high Zr ~700 ppm) as well as the interpolated age in the cores make it easy to correlate the  $39.85 \pm 0.14$  ka old (Giaccio et al., 2017) Campanian Ignimbrite from the Campi Flegrei (e.g., Federman & Carey, 1980; Tomlinson et al., 2015) with marine tephra layer CA8 (CI, Figures 7b, 7d and 9; Tables 1 and S3 in Data Set S1). We found this distal ash in cores POS 513–8, –9, –14, –15, –30, –31, –32, –35, –37, –40, –41, –45, –53, and –56 with thicknesses ranging from 3 to 14 cm (Figure 3c). CI distal ash has been found as layer Y-5 across most of the Mediterranean Sea (e.g., Engwell et al., 2014; Keller et al., 1978; Margari et al., 2007; Satow et al., 2020, 2015; Vinci, 1985; Wulf et al., 2020).

**Figure 12.** Stratigraphy of compositionally correlated tephra layers CA1 through CA20 in the 22 selected cores from the western part of the working area (CSK and Milos) arranged from W (left) to E (right) and on a horizontal line connecting CA3. Layers CA1 to CA20 correlate with tephra layers on land as shown in Figures 7–9. Ash layers are shaded gray and black, for felsic and mafic compositions, respectively; hemipelagic background sediment is shaded green, and brown layers represent sapropel intervals (cf. Rohling et al., 2015). Ash layers with a question mark could not be correlated. Green dots show the positions of the cores in a west to east transect, also representing the prevailing wind direction for ash fall distribution.

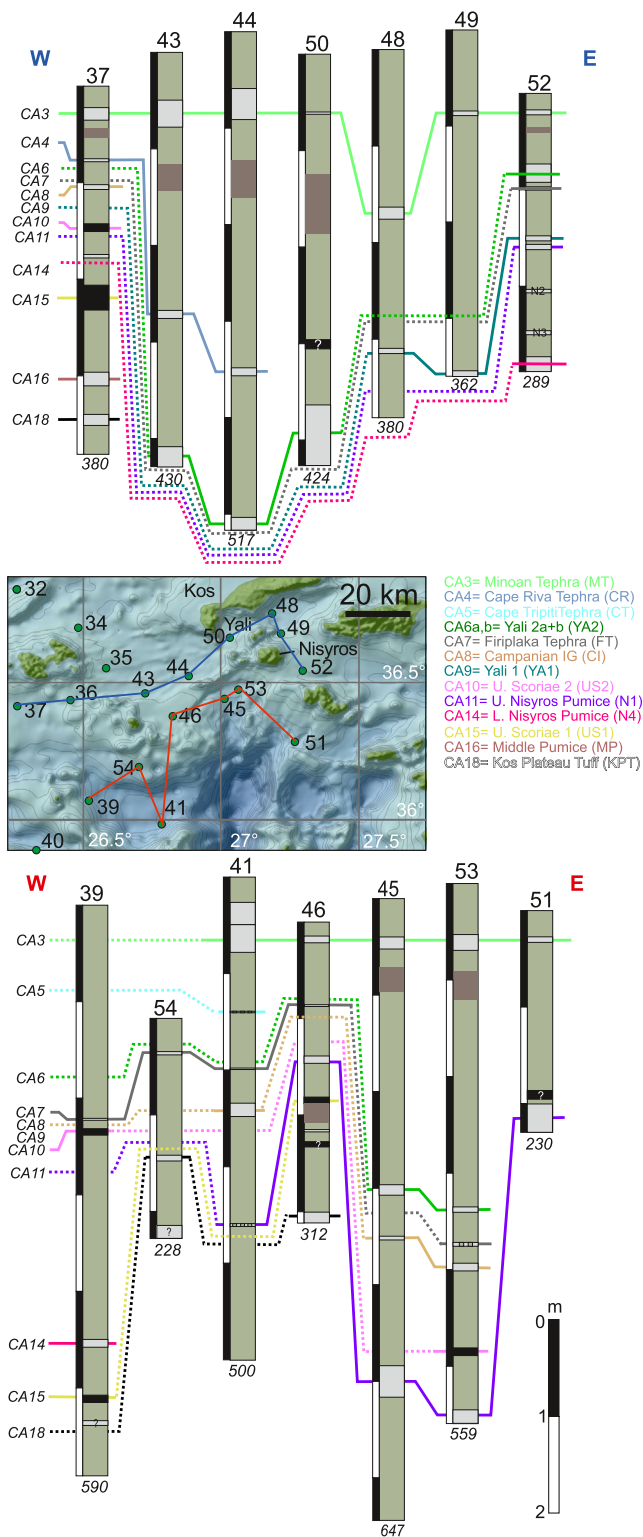


**Figure 13.** Continuation of Figure 12 in the eastern part of the working area in a west to east transect (Kos-Yali-Nisyros region).

### 6.3.8. Tephros From Unknown Sources

A number of ash beds have glass compositions that we cannot correlate with specific eruption products on the islands. However, following the example from the Central American volcanic arc (e.g., Carr et al., 2007, 2003; Kutterolf et al., 2008), systematic variations along the Aegean Volcanic Arc in geochemical parameters that are relatively insensitive to magmatic differentiation (Figure 11) can be used to attribute ash-bed compositions to specific regions of the arc. Where such compositional correlation is ambiguous, we favor the source area closest to core position considering the large distances between the Milos-CSK-KYN volcanic complexes.

There are three rhyolitic marine tephros in two cores west of Santorini and close to Milos (POS 513–7, and 8) of which the ash layer in POS 513–8 (507–511 cm bsf) correlates to an ash layer in core POS 513–7 (200–204 cm bsf) in terms of major and trace element glass compositions. The trace element compositions of these layers (red box in Figure 11) are not known from Santorini; some trace element ratios would fit Milos tephra compositions but others lie in-between the Milos and Santorini values.

Ash layers POS 513–46, 215–217 and POS 513–46, 227–232 cm bsf (green square and circle in Figure 11) have trace element ratios similar to the Kyra pyroclastics on Nisyros and an estimated age of ~120 ka (see part 2) that fits to the given eruptive age, but Ba/Y for example, is too low and also other trace element ratios are close but do not directly match the available onshore composition of Kyra pyroclastics (Table S3 in Data Set S1). Therefore this correlation remains uncertain.

Ash layer POS513-15, 196–206 cm bsf (black triangle in Figure 11) has trace element ratios similar to Kolumbo 1650 tephra but an estimated age of ~20 ka (see part 2), which does not fit. Proximity to Kolumbo Volcano suggests POS 513–15, 196–206 cm bsf came from an older eruption of Kolumbo but without any other constraints this correlation remains uncertain.

Ash layers POS 513–39, 533–538 cm bsf and POS 513–36, 286–293 cm bsf (yellow tilted triangles in Figure 11), and POS 513–51, 187–196 cm bsf (yellow hexagons in Figure 11) have unique major and trace element compositions (59.2–61.4 wt% SiO<sub>2</sub>, 1.6 to 2.6 wt% K<sub>2</sub>O), but ages based on sedimentation rates between 80 and 150 ka indicate different eruptions (see Part 2). Together with POS 513–50, 295–300 cm bsf (48.9 wt% SiO<sub>2</sub>, 1.5 wt% K<sub>2</sub>O), these samples have very high Nb/U that does not match any Aegean Volcanic Arc composition (Figure 11). Also, together with the basaltic to andesitic major element compositions, these samples do not correlate with tephra compositions of this age range known so far from the Anatolian Arc (e.g., Schmincke & Sumita, 2014; Tomlinson et al., 2015; Tryon et al., 2009).

## 7. Conclusions

We have established a new reference data base of glass compositions, particularly including trace element glass compositions, of stratigraphically controlled widespread, mostly plinian tephros from land that have been erupted during the last ~200 kyrs along the Aegean Volcanic Arc. This data base enabled us to correlate 209 ash layers in sediment gravity cores collected during marine cruise POS 513 in the Aegean Sea to 19 eruptions from the Aegean Volcanic Arc, resulting in a tephrostratigraphy for medial to distal sediment cores (Figures 12 and 13).

We achieved correlations with 11 major tephra from the CSK volcanic complex (Kameni, Kolumbo 1650, Minoan, Cape Riva, Cape Tripiti, Upper Scoriae 1 and 2, Middle Pumice, Cape Thera, Lower Pumice, Cape Therma 3). Contrary to expectation, considering the proximity of some of our cores to Santorini, we found no clear evidence of the inter-plinian events in the seafloor cores, which may either be due to the present unavailability of trace element glass compositions of the inter-plinian deposits or to easy erosion or bioturbation of such presumably very thin ash beds. However, fine ashes from such smaller eruptions are potentially preserved as cryptotephra in the sediments, which we have not investigated in this study but which may be addressed in dedicated future studies.

We have also discovered new tephra not previously known from land. One is a widespread tephra from Milos which was not previously known to have produced such deposits. The others are two tephra from Nisyros that lie bracketed between the marine equivalents of Upper and Lower Pumice on the island. Including also correlations to the Kos Plateau Tuff and Yali 1 and 2 tephra, all our correlations provide a tephrostratigraphic grid between the volcanic centers from Milos to Nisyros (Figures 12 and 13).

### Data Availability Statement

All data produced during this study and defining the core and onland sample locations is under way at Kutterolf, Freundt, Hansteen, et al., 2021 in PANGAEA Data Archiving and Publication (<https://doi.org/10.1594/PANGAEA.938615>). An electronic copy of this data file is provided as Tables S1–S5 in Data Set S1.

### Acknowledgments

The RV POSEIDON cruise POS 513 in 2017 was financed by GEOMAR Helmholtz Centre for Ocean Research Kiel. We are particularly grateful for the excellent support and hospitable atmosphere during the cruise provided by Captain Volland and his entire crew. Moreover, we appreciate very much the enthusiastic hard work of all members of the scientific party. We thank the captain and the crew of the E/V Nautilus for their excellent support during the execution of cruise NA-007. We also appreciate the review by S. Wulf which helped to improve this paper. This is Laboratory of Excellence ClerVolc Contribution Number 504. Open access funding enabled and organized by Projekt DEAL.

### References

- Aarbourg, S., & Frechen, M. (1999). *Die pyroklastischen Abfolgen der Christiana-Inseln (Süd-Ägäis, Griechenland)* (pp. 260–276). *Terrestrische Quartärgeologie*.
- Aksu, A. E., Jenner, G., Hiscott, R. N., & Isler, E. B. (2008). Occurrence, stratigraphy and geochemistry of Late Quaternary tephra layers in the Aegean Sea and the Marmara Sea. *Marine Geology*, 252, 174–192. <https://doi.org/10.1016/j.margeo.2008.04.004>
- Allen, S. R., & Cas, R. A. F. (1998). Rhyolitic fallout and pyroclastic density current deposits from a phreatoplinian eruption in the eastern Aegean Sea, Greece. *Journal of Volcanology and Geothermal Research*, 86, 219–251. [https://doi.org/10.1016/S0377-0273\(98\)00080-8](https://doi.org/10.1016/S0377-0273(98)00080-8)
- Allen, S. R., & Cas, R. A. F. (2001). Transport of pyroclastic flows across the sea during the explosive, rhyolitic eruption of the Kos Plateau Tuff, Greece. *Bulletin of Volcanology*, 62, 441–456. <https://doi.org/10.1007/s004450000107>
- Allen, S. R., & McPhie, J. (2000). Water-settling and resedimentation of submarine rhyolitic pumice at Yali, eastern Aegean, Greece. *Journal of Volcanology and Geothermal Research*, 95, 285–307. [https://doi.org/10.1016/S0377-0273\(99\)00127-4](https://doi.org/10.1016/S0377-0273(99)00127-4)
- Allen, S. R., Stadlbauer, E., & Keller, J. (1999). Stratigraphy of the Kos Plateau Tuff: Product of a major Quaternary explosive rhyolitic eruption in the eastern Aegean, Greece. *International Journal of Earth Sciences*, 88, 132–156. <https://doi.org/10.1007/s005310050251>
- Andújar, J., Scaillet, B., Pichavant, M., & Druitt, T. H. (2016). Generation conditions of Dacite and Rhyodacite via the crystallization of an Andesitic magma. Implications for the plumbing system at Santorini (Greece) and the origin of tholeiitic or calc-alkaline differentiation trends in arc magmas. *Journal of Petrology*, 57(10), 1887–1920. <https://doi.org/10.1093/ptrology/egw061>
- Bachmann, O., Deering, C. D., Ruprecht, J. S., Huber, C., Skopelitis, A., & Schnyder, C. (2012). Evolution of silicic magmas in the Kos-Nisyros volcanic center, Greece: A petrological cycle associated with caldera collapse. *Contributions to Mineralogy and Petrology*, 163, 151–166. <https://doi.org/10.1007/s00410-011-0663-y>
- Bohnhoff, M., Rische, M., Meier, T., Becker, D., Stavrakakis, G., & Harjes, H.-P. (2006). Microseismic activity in the Hellenic Volcanic Arc, Greece, with emphasis on the seismotectonic setting of the Santorini-Amorgos zone. *Tectonophysics*, 423, 17–33. <https://doi.org/10.1016/j.tecto.2006.03.024>
- Bonneau, M., & Kienast, J. R. (1982). Subduction, collision et schistes bleus: Exemple de l'Égée, Grèce. *Bulletin Société Géologie France*, 7, 785–791. <https://doi.org/10.2113/gssgfbull.s7-xxiv.4.785>
- Bronk Ramsey, C., Albert, P. G., Blockley, S. P. E., Hardiman, M., Houley, R. A., Lane, C. S., et al. (2015). Improved age estimates for key Late Quaternary European tephra horizons in the RESET lattice. *Quaternary Science Reviews*, 118, 18–32. <https://doi.org/10.1016/j.quascirev.2014.11.007>
- Cambray, H., Cadet, J.-P., & Poulet, A. (1993). Ash layers in deep-sea sediments as tracers of arc volcanic activity: Japan and Central America as case studies. *Island Arc*, 2(2), 72–86. <https://doi.org/10.1111/j.1440-1738.1993.tb00075.x>
- Campos Venuti, M., & Rossi, R. L. (1996). Depositional facies in the Firiplaka rhyolitic Tuff Ring, Milos Island (Cyclades, Greece). *Acta Vulcanologica*, 8(2), 47–63.
- Cantner, K., Carey, S., & Nomikou, P. (2014). Integrated volcanologic and petrologic analysis of the 1650 AD eruption of Kolumbo submarine volcano, Greece. *Journal of Volcanology and Geothermal Research*, 269, 28–43. <https://doi.org/10.1016/j.jvolgeoes.2013.10.004>
- Carey, S., Nomikou, P., Croff Bell, K., & Ballard, D. (2013). Exploration of the Santorini volcanic group, southern Aegean Sea. *Oceanography (Washington, D.C.)*, 26(no. 1 supplement), 44–49.
- Carey, S., Nomikou, P., Croff Bell, K., Lilley, M., Lupton, J., Roman, C., et al. (2013). CO<sub>2</sub> degassing from hydrothermal vents at Kolumbo submarine volcano, Greece, and the accumulation of acidic crater water. *Geology*, 41, 1035–1038. <https://doi.org/10.1130/g34286.1>
- Carr, M. J., Feigenson, M. D., Patino, L. C., & Walker, J. A. (2003). Volcanism and geochemistry in Central America: Progress and problems. In J. Eiler (Ed.), *Inside the Subduction Factory, Geophysical Monograph Series* (Vol. 138, pp. 153–174). AGU. <https://doi.org/10.1029/138gm09>
- Carr, M. J., Patino, L. C., & Feigenson, M. D. (2007). Petrology and geochemistry of lavas. In J. Buntschuh, & G. E. Alvarado (Eds.), *Central America—Geology, Resources and Hazards* (Vol. 2, pp. 565–590). A. A. Balkema.
- Cassidy, M., Watt, S. F. L., Palmer, M. R., Trofimovs, J., Symons, W., Maclachlan, S. E., & Stinton, A. J. (2014). Construction of volcanic records from marine sediment cores: A review and case study (Montserrat, West Indies). *Earth-Science Reviews*, 138, 137–155. <https://doi.org/10.1016/j.earscirev.2014.08.008>

- Clift, P. D., & Blusztajn, J. (1999). The trace-element characteristics of Aegean and Aeolian volcanic arc marine tephra. *Journal of Volcanology and Geothermal Research*, 92, 321–347. [https://doi.org/10.1016/s0377-0273\(99\)00059-1](https://doi.org/10.1016/s0377-0273(99)00059-1)
- Dewey, J. F., & Sengör, A. M. C. (1979). Aegean and surrounding regions: Complex multiplate and continuum tectonics in a convergent zone. *The Geological Society of America Bulletin*, 90, 84–92. [https://doi.org/10.1130/0016-7606\(1979\)90<84:aasrcm>2.0.co;2](https://doi.org/10.1130/0016-7606(1979)90<84:aasrcm>2.0.co;2)
- Dietrich, V. J., & Lagios, E. (2018). *Nisyros volcano, active volcanoes of the world* (pp. 13–55). Hardcover (ISBN: 978-3-319-55458-7).
- Druitt, T. H. (2014). New insights into the initiation and venting of the Bronze-Age eruption of Santorini (Greece), from component analysis. *Bulletin of Volcanology*, 76, 794. <https://doi.org/10.1007/s00445-014-0794-x>
- Druitt, T. H., Edwards, L., Mellors, R. A., Pyle, D. M., Sparks, R. S. J., Lanphere, M., et al. (1999). *Santorini Volcano* (Vol. 19, p. 165). Geological Society London Memoirs.
- Druitt, T. H., & Francaviglia, V. (1992). Caldera formation on Santorini and the physiography of the islands in the late Bronze Age. *Bulletin of Volcanology*, 54, 484–493. <https://doi.org/10.1007/bf00301394>
- Druitt, T. H., Mellors, R. A., Pyle, D. M., & Sparks, R. S. J. (1989). Explosive volcanism on Santorini, Greece. *Geological Magazine*, 126, 95–126. <https://doi.org/10.1017/s001675680006270>
- Druitt, T. H., Mercier, M., Florentin, L., Delouie, E., Cluzel, N., Flaherty, T., et al. (2016). Magma storage and extraction associated with plinian and inter-plinian activity at Santorini Caldera (Greece). *Journal of Petrology*, 57, 461–494. <https://doi.org/10.1093/petrology/egw015>
- Engwell, S. L., Sparks, R. S. J., & Carey, S. (2014). Physical characteristics of tephra layers in the deep sea realm: The Campanian Ignimbrite eruption. In Austin WEN, P. M. Abbott, S. M. Davies, N. J. G. Pearce, & S. Wastegard (Eds.), *Marine Tephrochronology* (Vol. 398, pp. 47–64). Geological Society, London, Special Publications. <https://doi.org/10.1144/SP398.7>
- Fabbro, G. N., Druitt, T. H., & Scaillet, S. (2013). Evolution of the crustal magma plumbing system during the build-up to the 22-ka caldera-forming eruption of Santorini (Greece). *Bulletin of Volcanology*, 75, 767. <https://doi.org/10.1007/s00445-013-0767-5>
- Federman, A. N., & Carey, S. N. (1980). Electron microprobe correlation of tephra from eastern Mediterranean abyssal sediments and the island of Santorini. *Quaternary Research*, 13, 160–171. [https://doi.org/10.1016/0033-5894\(80\)90026-5](https://doi.org/10.1016/0033-5894(80)90026-5)
- Fouqué, F. A. (1879). *Santorini and its eruptions (translated and annotated by A.R. McBirney, 1998)*. Johns Hopkins University Press.
- Francalanci, L., Varekamp, J. C., Vougioukalakis, G., Defant, M. J., Innocenti, F., & Manetti, P. (1995). Crystal retention, fractionation and crustal assimilation in a convecting magma chamber, Nisyros Volcano, Greece. *Bulletin of Volcanology*, 56, 601–620. <https://doi.org/10.1007/bf00301465>
- Francalanci, L., Vougioukalakis, G. E., Perini, G., & Manetti, P. (2005). A west-east traverse along the magmatism of the south Aegean volcanic arc in the light of volcanological, chemical and isotopic data. In M. Fytikas, & G. E. Vougioukalakis (Eds.), *The south aegean active volcanic arc* (pp. 64–112). Elsevier.
- Freundt, A. (2017). *POS 513 cruise report* (p. 18). GEOMAR. [https://doi.org/10.3289/cr\\_pos513](https://doi.org/10.3289/cr_pos513)
- Freundt, A., Schindlbeck-Belo, J. C., Kutterolf, S., & Hopkins, J. L. (2021). Tephra layers in the marine environment: A review of properties and emplacement processes (pp. 520–2021). In A. Di Capua, R. De Rosa, G. Kereszturi, E. Le Pera, M. Rosi, S. F. L. Watt (Eds.), *Volcanic Processes in the Sedimentary Record: When Volcanoes Meet the Environment*. Geological Society, London, Special Publications, 520. <https://doi.org/10.1144/SP520-2021-50>
- Fujioka, K. (1986). Synthesis of Neogene explosive volcanism of the Tohoku arc, deduced from marine tephra drilled around the Japan Trench region. Deep Sea Drilling Project Legs 56, 57, and 87B, In *Initial Reports Deep Sea Drilling Project* (Vol. 587, pp. 703–726).
- Fuller, S., Carey, S., & Nomikou, P. (2018). Distribution of fine-grained tephra from the 1650 CE submarine eruption of Kolumbo. *Journal of Volcanology and Geothermal Research*, 352, 10–25. <https://doi.org/10.1016/j.jvolgeores.2018.01.004>
- Fytikas, M., Innocenti, F., Kolios, N., Manetti, P., Mazzuoli, R., Poli, G., et al. (1986). Volcanology and petrology of volcanic products from the island of Milos and neighbouring islets. *Journal of Volcanology and Geothermal Research*, 28, 297–317. [https://doi.org/10.1016/0377-0273\(86\)90028-4](https://doi.org/10.1016/0377-0273(86)90028-4)
- Giaccio, B., Hajdas, I., Isaia, R., Deino, A., & Nomade, S. (2017). High-precision <sup>14</sup>C and <sup>40</sup>Ar/<sup>39</sup>Ar dating of the Campanian Ignimbrite (Y-5) reconciles the time-scales of climatic-cultural processes at 40 ka. *Scientific Reports*, 7, 45940. <https://doi.org/10.1038/srep45940>
- Gertisser, R., Preece, K., & Keller, J. (2009). The Plinian Lower Pumice 2 Eruption, Santorini, Greece: Magma evolution and volatile behaviour. *Journal of Volcanology and Geothermal Research*, 186, 387–406.
- Günther, D., Jackson, S. E., & Longrich, H. P. (1999). Laser ablation and arc/spark solid sample introduction into inductively coupled plasma mass spectrometers. *Spectrochimica Acta Part B: Atomic Spectroscopy*, 54(3), 381–409.
- Hardiman, J. C. (1999). Deep sea tephra from Nisyros island, eastern Aegean Sea, Greece. In C. R. Firth, & W. J. McGuire (Eds.), *Volcanoes in the Quaternary* (Vol. 161, pp. 69–88). Geological Society London Special Publication. <https://doi.org/10.1144/gsl.sp.1999.161.01.06>
- Hieke, W., Hemleben, C., Linke, P., Türkay, M., & Weikert, H. (1999). Mittelmeer 1998/99, cruise No. 40, 28 October 1997–10 February 1998. In *METEOR-Berichte* (Vol. 99–2, pp. 1–301). Leitstelle METEOR, Institut für Meereskunde der Universität Hamburg. [https://doi.org/10.2312/cr\\_m40](https://doi.org/10.2312/cr_m40)
- Hoof, E. E. E., Nomikou, P., Toomey, D. R., Lampridou, D., Getz, C., Christopoulou, M.-E., et al. (2017). Backarc tectonism, volcanism, and mass wasting shape seafloor morphology in the Santorini-Christiana-Amorgos region of the Hellenic Volcanic Arc. *Tectonophysics*, 712–713, 396–414. <https://doi.org/10.1016/j.tecto.2017.06.005>
- Hopkins, J. L., Wysoczanski, R. J., Orpin, A. R., Howarth, J. D., Strachan, L. J., Lunenburg, R., et al. (2020). Deposition and preservation of tephra in marine sediments at the active Hikurangi subduction margin. *Quaternary Science Reviews*, 247, 106500. <https://doi.org/10.1016/j.quascirev.2020.106500>
- Hunt, J. B., & Hill, P. G. (2001). Tephrological implications of beam sized sample-size effects in electron microprobe analysis of glass shards. *Journal. Quaternary Sciences*, 16, 105e117. <https://doi.org/10.1002/jqs.571>
- Hunt, J. B., & Najman, Y. M. R. (2003). Tephrochronological and tephrostratigraphical potential of Pliocene-Pleistocene volcaniclastic deposits in the Japan Forearc, ODP Leg 186. In K. Suyehiro, I. S. Sacks, G. D. Acton, & M. Oda (Eds.), *Proceedings of the Ocean Drilling Program, Scientific Results* (Vol. 186). <https://doi.org/10.2973/odp.proc.sr.2186.2107.2003>
- Hübscher, C., Ruhnau, M., & Nomikou, P. (2015). Volcano-tectonic evolution of the polygenetic Kolumbo submarine volcano/Santorini (Aegean Sea). *Journal of Volcanology and Geothermal Research*, 291, 101–111.
- Jackson, J. A. (1994). Active tectonics of the Aegean region. *Annual Review of Earth and Planetary Sciences*, 22, 239–271. <https://doi.org/10.1146/annurev.earth.22.050194.001323>
- Jarosewich, E., Nelen, J., & Norberg, J. A. (1980). Reference samples for electron microprobe analysis. *Geostandards Newsletter*, 4, 43–47. <https://doi.org/10.1111/j.1751-908x.1980.tb00273.x>
- Johnston, E. N., Sparks, R. S. J., Phillips, J. C., & Carey, S. (2014). Revised estimates for the volume of the Late Bronze Age Minoan eruption, Santorini, Greece. *Journal Geological Society London*, 171, 583–590. <https://doi.org/10.1144/jgs2013-113>

- Karkanias, P., White, D., Lane, C. S., Stringer, C., Davies, W., Cullen, V. L., et al. (2015). Tephra correlations and climatic events between the MIS6/5 transition and the beginning of MIS3 in Theopetra Cave, central Greece. *Quaternary Science Reviews*, *118*, 170–181. <https://doi.org/10.1016/j.quascirev.2014.05.027>
- Keller, J., Gertisser, R., Reusser, E., & Dietrich, V. (2014). Pumice deposits of the Santorini Lower Pumice 2 eruption on Anafi island, Greece: Indications for a Plinian event of exceptional magnitude. *Geochemistry, Geophysics, Geosystems*, *278–279*, 120–128. <https://doi.org/10.1016/j.jvolgeores.2014.04.009>
- Keller, J., Rehren, T. H., & Stadlbauer, E. (1990). Explosive volcanism in the Hellenic Arc: A summary and review. In D. A. Hardy, J. Keller, V. P. Galanopoulos, N. C. Flemming, & T. H. Druitt (Eds.), *Thera and the Aegean World III. Proceedings of the third International Congress on the Volcano of Thera* (pp. 13–26).
- Keller, J., Ryan, W. B. F., Ninkovich, D., & Altherr, R. (1978). Explosive volcanic activity in the Mediterranean over the past 200,000 years as recorded in deep-sea sediments. *The Geological Society of America Bulletin*, *89*, 591–604. [https://doi.org/10.1130/0016-7606\(1978\)89<591:evaitm>2.0.co;2](https://doi.org/10.1130/0016-7606(1978)89<591:evaitm>2.0.co;2)
- Kiliass, S. P., Nomikou, P., Papanikolaou, D., Polymenakou, P. N., Godelitsas, A., Argyraki, A., et al. (2013). New insights into hydrothermal vent processes in the unique shallow-submarine arc-volcano, Kolumbo (Santorini), Greece. *Scientific Reports*, *3*, 2421. <https://doi.org/10.1038/srep02421>
- Kutterolf, S., Freundt, A., & Burkert, C. (2011). Eruptive history and magmatic evolution of the 1.9 ka Plinian dacitic Chiltepe Tephra from Apoyeque volcano in west-central Nicaragua. *Bulletin Volcanology*, *73*, 811–831. <https://doi.org/10.1007/s00445-011-0457-0>
- Kutterolf, S., Freundt, A., Druitt, T., McPhie, J., Nomikou, P., Pank, P., et al. (2021). The medial offshore record of explosive volcanism along the Central to Eastern Aegean Arc, part 2: Tephra ages and volumes, eruption magnitudes and marine sedimentation rate variations, *Geochemistry, Geophysics, Geosystems*. <https://doi.org/10.1029/2021GC010011>
- Kutterolf, S., Freundt, A., Hansteen, T. H., Dettbarn, R., Hampel, F., Sievers, C., et al. (2021). Major and trace elements of Aegean Arc tephra. *PANGAEA*. <https://doi.org/10.1594/PANGAEA.937928>
- Kutterolf, S., Freundt, A., Peréz, W., Mörz, T., Schacht, U., Wehrmann, H., & Schmincke, H. U. (2008). Pacific offshore record of plinian arc volcanism in Central America: 1. Along-arc correlations. *Geochemistry, Geophysics, Geosystems*, *9*, Q02S01. <https://doi.org/10.1029/2007GC001631>
- Le Maitre, R. W., Streckeis, A., Zanettin, B., Le Bas, M. J., Bonin, B., & Bateman, P. (2002). *Igneous rocks: A classification and glossary of terms*. Cambridge University Press.
- Le Pichon, X., & Kreemer, C. (2010). The miocene-to-present kinematic evolution of the Eastern Mediterranean and Middle East and its implications for dynamics. *Annual Review of Earth and Planetary Sciences*, *38*, 323–351. <https://doi.org/10.1146/annurev-earth-040809-152419>
- Limburg, E. M., & Varecamp, J. C. (1991). Young pumice deposits on Nisyros, Greece. *Bulletin of Volcanology*, *54*, 68–77. <https://doi.org/10.1007/bf00278207>
- Longchamp, C., Bonadonna, C., Bachmann, O., & Skopelitis, A. (2011). Characterization of tephra deposits with limited exposure: The example of the two largest explosive eruptions at Nisyros volcano (Greece). *Bulletin of Volcanology*, *73*, 1337–1352. <https://doi.org/10.1007/s00445-011-0469-9>
- Margari, V., Pyle, D. M., Bryant, C., & Gibbard, P. L. (2007). Mediterranean tephra stratigraphy revisited: Results from a long terrestrial sequence on Lesbos Island, Greece. *Journal of Volcanology and Geothermal Research*, *163*, 34–54. <https://doi.org/10.1016/j.jvolgeores.2007.02.002>
- Mazzullo, J., & Graham, A. G. (1988). Handbook for shipboard sedimentologists. *Ocean Drilling Program Technical Note*, *8*, 67. <https://doi.org/10.2973/odp.tn.8.1988>
- McCoy, F. W. (1981). Areal distribution, redeposition and mixing of tephra within deep-sea sediments of the Eastern Mediterranean sea. In S. Self, & R. S. J. Sparks (Eds.), *Tephra studies. Nato advanced study Institutes series C 75* (pp. 245–254). Reidel. [https://doi.org/10.1007/978-94-009-8537-7\\_15](https://doi.org/10.1007/978-94-009-8537-7_15)
- McCoy, F. W., & Heiken, G. (2000). *The Late-Bronze Age Explosive Eruption of Thera (Santorini), Greece: Regional and Local Effects* (Vol. 345, pp. 43–70). Geological Society America Special Paper. <https://doi.org/10.1130/0-8137-2345-0-43>
- McKenzie, D. P. (1972). Active tectonics of the Mediterranean region. *Geophysical Journal of the Royal Astronomical Society*, *30*, 109–185. <https://doi.org/10.1111/j.1365-246x.1972.tb02351.x>
- Narcisi, B., & Vezzoli, L. (1999). Quaternary stratigraphy of distal tephra layers in the Mediterranean-An overview. *Global and Planetary Change*, *21*, 31–50. [https://doi.org/10.1016/s0921-8181\(99\)00006-5](https://doi.org/10.1016/s0921-8181(99)00006-5)
- Newman, A. V., Stiros, S., Feng, L., Psimoulis, P., Moschas, F., Saltogianni, V., et al. (2012). Recent geodetic unrest at Santorini Caldera, Greece. *Geophysical Research Letters*, *39*, L06309. <https://doi.org/10.1029/2012GL051286>
- Nomikou, P., Carey, S., Croff Bell, K., Papanikolaou, D., Bejelou, K., Cantner, K., et al. (2012). Tsunami hazard risk of a future volcanic eruption of Kolumbo submarine volcano, NE of Santorini Caldera, Greece. *Natural Hazards*, *72*, 1375–1390. <https://doi.org/10.1007/s11069-012-0405-0>
- Nomikou, P., Carey, S., Papanikolaou, D., Croff Bell, K., Sakellariou, D., Alexandri, M., et al. (2013). Morphological analysis and related volcanic features of the Kolumbo submarine volcanic chain (NE of Santorini Island, Aegean volcanic arc). *Zeitschrift für Geomorphologie*, *57*, 29–47. <https://doi.org/10.1127/0372-8854/2013/s-00142>
- Nomikou, P., Carey, S., Papanikolaou, D., Croff Bell, K. L., Sakellariou, D., Alexandri, M., & Bejelou, K. (2012). Submarine volcanoes of the Kolumbo volcanic zone NE of Santorini Caldera, Greece. *Global and Planetary Change*, *90–91*, 135–151. <https://doi.org/10.1016/j.gloplacha.2012.01.001>
- Nomikou, P., Druitt, T. H., Hübscher, C., Mather, T. A., Paulatto, M., Kalnins, L. M., et al. (2016). Post-eruptive flooding of Santorini caldera and implications for tsunami generation. *Nature Communications*, *7*, 13332. <https://doi.org/10.1038/ncomms13332>
- Nomikou, P., Hübscher, C., & Carey, S. (2019). The Christiana–Santorini–Kolumbo Volcanic Field. *Elements*, *15*(3), 171–176. <https://doi.org/10.2138/gselements.15.3.171>
- Nomikou, P., Hübscher, C., Papanikolaou, D., Farangitakis, P. G., Ruhnu, M., & Lampridou, D. (2018). Expanding extension, subsidence and lateral segmentation within the Santorini-Amorgos basins during Quaternary: Implications for the 1956 Amorgos events, central-South Aegean Sea, Greece. *Tectonophysics*, *722*, 138–153. <https://doi.org/10.1016/j.tecto.2017.10.016>
- Nomikou, P., Hübscher, C., Ruhnu, M., & Bejelou, K. (2016). Tectono-stratigraphic evolution through successive extensional events of the Andros Basin, hosting Kolumbo volcanic field at the Aegean. *Tectonophysics*, *671*, 202–217. <https://doi.org/10.1016/j.tecto.2016.01.021>
- Nomikou, P., & Papanikolaou, D. (2011). Extension of active fault zones on Nisyros volcano across the Yali-Nisyros Channel based on onshore and offshore data. *Marine Geophysical Researches*, *32*, 181–192. <https://doi.org/10.1007/s11001-011-9119-z>
- Nomikou, P., Papanikolaou, D., Alexandri, M., Sakellariou, D., & Rousakis, G. (2013). Submarine volcanoes along the Aegean volcanic arc. *Tectonophysics*, *597–598*, 123–146. <https://doi.org/10.1016/j.tecto.2012.10.001>
- Nomikou, P., Papanikolaou, D., & Dietrich, V. J. (2018). Geodynamics and Volcanism in the Kos-Yali-Nisyros Volcanic Field. In V. Dietrich, & E. Lagios (Eds.), *Nisyros volcano. Active volcanoes of the World* (pp. 13–55). Springer. [https://doi.org/10.1007/978-3-319-55460-0\\_2](https://doi.org/10.1007/978-3-319-55460-0_2)

- Nomikou, P., Parks, M. M., Papanikolaou, D., Pyle, D. M., Mather, T. A., Carey, S., et al. (2014). The emergence and growth of a submarine volcano: The Kameni islands, Santorini (Greece). *Geological Research*, *1*, 1–2, 8–18. <https://doi.org/10.1016/j.grj.2014.02.002>
- Norman, M., Pearson, N., Sharma, A., & Griffin, W. (1996). Quantitative analysis of trace elements in geological materials by laser ablation ICPMS: Instrumental operating conditions and calibration values of NIST glasses. *Geostandards Newsletter*, *20*(2), 247–261. <https://doi.org/10.1111/j.1751-908x.1996.tb00186.x>
- Papadopoulos, G. A., Sachpazi, M., Panopoulou, G., & Stavrakakis, G. (1998). The volcanoseismic crisis of 1996–97 in Nisyros, SE Aegean Sea, Greece. *Terra Nova*, *10*, 151–154. <https://doi.org/10.1046/j.1365-3121.1998.00184.x>
- Papanikolaou, D., & Nomikou, P. (2001). Tectonic structure and volcanic centres at the eastern edge of the Aegean volcanic arc around Nisyros Island. *Bulletin of the Geological Society of Greece*, *34*(1), 289–296. <https://doi.org/10.12681/bgs.17025>
- Papazachos, B. C., Dimitriadis, S. T., Panagiotopoulos, D. G., Papazachos, C. B., & Papadimitriou, E. E. (2005). Deep structure and active tectonics of the southern Aegean volcanic arc. In M. Fytikas, & G. E. Vougioukalakis (Eds.), *The South Aegean active volcanic arc* (pp. 4–64). Elsevier. [https://doi.org/10.1016/s1871-644x\(05\)80032-4](https://doi.org/10.1016/s1871-644x(05)80032-4)
- Parks, M. M., Biggs, J., England, P., Mather, T. A., Nomikou, P., Palamartchouk, K., et al. (2012). Evolution of Santorini Volcano dominated by episodic and rapid fluxes of melt from depth. *Nature Geoscience*, *5*(10), 749–754. <https://doi.org/10.1038/ngeo1562>
- Peccerillo, R., & Taylor, S. R. (1976). Geochemistry of Eocene calc-alkaline volcanic rocks from the Kastamonu area, northern Turkey. *Contributions to Mineralogy and Petrology*, *58*, 63–81. <https://doi.org/10.1007/bf00384745>
- Pe-Piper, G., & Piper, D. J. W. (2005). The South Aegean active volcanic arc: Relationships between magmatism and tectonics. *Developments in Volcanology*, *7*, 113–133. [https://doi.org/10.1016/s1871-644x\(05\)80034-8](https://doi.org/10.1016/s1871-644x(05)80034-8)
- Piper, D. J. W., & Peirssonatis, C. (2003). Quaternary neotectonics of the South Aegean arc. *Marine Geology*, *198*, 259–288. [https://doi.org/10.1016/s0025-3227\(03\)00118-x](https://doi.org/10.1016/s0025-3227(03)00118-x)
- Popa, R.-G., Guillong, M., Bachmann, O., Szymanowski, D., & Ellis, B. (2020). U-Th zircon dating reveals a correlation between eruptive styles and repose periods at the Nisyros-Yali volcanic area, Greece. *Chemical Geology*, *555*, 119830. <https://doi.org/10.1016/j.chemgeo.2020.119830>
- Pyle, D. M. (1990). New estimates for the volume of the Minoan eruption. In D. A. Hardy, & A. C. Renfrew (Eds.), *Thera and the Aegean world III: Volume 2 earth sciences* (pp. 113–121). The Thera Foundation.
- Pyle, D. M., & Elliott, J. R. (2006). Quantitative morphology, recent evolution, and future activity of the Kameni islands volcano, Santorini, Greece. *Geosphere*, *2*, 253–268. <https://doi.org/10.1130/ges00028.1>
- Rinaldi, M., & Campos Venuti, M. (2003). The submarine eruption of the Bombarda volcano, Milos Island, Cyclades, Greece. *Bulletin of Volcanology*, *65*, 282–293. <https://doi.org/10.1007/s00445-002-0260-z>
- Rohling, E. J., Marino, G., & Grant, K. M. (2015). Mediterranean climate and oceanography, and the periodic development of anoxic events (sapropels). *Earth-Science Reviews*, *143*, 62–97. <https://doi.org/10.1016/j.earscirev.2015.01.008>
- Royden, L. H., & Papanikolaou, D. J. (2011). Slab segmentation and late Cenozoic disruption of the Hellenic arc. *Geochemistry, Geophysics, Geosystems*, *12*, Q03010. <https://doi.org/10.1029/2010GC003280>, doi.org/
- Ryan, W. B. F., Carbotte, S. M., Coplan, J. O., O'Hara, S., Melkonian, A., Arko, R., et al. (2009). Global multi-resolution topography synthesis. *Geochemistry, Geophysics, Geosystems*, *10*, Q03014. <https://doi.org/10.1029/2008GC002332>
- Satow, C., Grant, K. M., Wulf, S., Schulz, H., Mallon, A., Matthews, I., & Lowe, J. (2020). Detection and characterisation of Eemian Marine Tephra layers within the sapropel s5 sediments of the Aegean and Levantine Seas. *Quaternary*, *3*, 6. <https://doi.org/10.3390/quat3010006>
- Satow, C., Tomlinson, E. L., Grant, K. M., Albert, P. G., Smith, V. C., Manning, C. J., et al. (2015). A new contribution to the Late Quaternary tephratigraphy of the Mediterranean: Aegean Sea core LC21. *Quaternary Science Reviews*, *117*, 96–112. <https://doi.org/10.1016/j.quascirev.2015.04.005>
- Schindlbeck, J. C., Kutterolf, S., Freundt, A., Alvarado, G. E., Wang, K. L., Straub, S. M., et al. (2016). Late Cenozoic tephratigraphy offshore the southern Central American Volcanic Arc: 1. Tephra ages and provenance. *Geochemistry, Geophysics, Geosystems*, *17*, 4641–4668. <https://doi.org/10.1002/2016GC006503>
- Schindlbeck, J. C., Kutterolf, S., Freundt, A., Scudder, R. P., Pickering, K. T., & Murray, R. W. (2013). Emplacement processes of submarine volcanoclastic deposits (IODP Site C0011, Nankai Trough). *Marine Geology*, *343*, 115–124. <https://doi.org/10.1016/j.margeo.2013.06.017>
- Schmincke, H. U., & Sumita, M. (2014). Impact of volcanism on the evolution of Lake Van (eastern Anatolia) III: Periodic (Nemrut) vs. episodic (Süphan) explosive eruptions and climate forcing reflected in a tephra gap between ca. 14 ka and ca. 30 ka. *Journal of Volcanology and Geothermal Research*, *285*, 195–213. <https://doi.org/10.1016/j.jvolgeores.2014.08.015>
- Schneider, J. L., Le Ruyet, A., Chanier, F., Buret, C., Ferriere, J., Proust, J. N., & Rosseel, J. B. (2001). Primary or secondary distal volcanoclastic turbidites: How to make the distinction? An example from the Miocene of New Zealand (Mahia Peninsula, North Island). *Sedimentary Geology*, *145*, 1–22. [https://doi.org/10.1016/s0037-0738\(01\)00108-7](https://doi.org/10.1016/s0037-0738(01)00108-7)
- Schwarz, M. (2000). *Tephra Korrelation im östlichen Mittelmeer (Meteor M40/4 Kerne)*. Diploma thesis (p. 257). Albert-Ludwigs-Universität Freiburg.
- Shaw, B., & Jackson, J. (2010). Earthquake mechanisms and active tectonics of the Hellenic subduction zone. *Geophysical Journal International*, *181*, 966–984. <https://doi.org/10.1111/j.1365-246x.2010.04551.x>
- Sigurdsson, H., Carey, S., Alexandri, G., Vougioukalakis, G., Croff, K., Roman, C., et al. (2006). Marine investigations of Greece's Santorini volcanic field. *EOS Trans Am Geophys Union*, *87*(337), 342. <https://doi.org/10.1029/2006eo340001>
- Simmons, J. M., Cas, R. A. F. F., Druitt, T. H., & Carey, R. J. (2017). The initiation and development of a caldera-forming Plinian eruption (172ka Lower Pumice 2 eruption, Santorini, Greece). *Journal of Volcanology and Geothermal Research*, *341*, 332–350. <https://doi.org/10.1016/j.jvolgeores.2017.05.034>
- Simmons, J. M., Cas, R. A. F. F., Druitt, T. H., & Folkes, C. B. (2016). Complex variations during a caldera-forming Plinian eruption, including precursor deposits, thick pumice fallout, co-ignimbrite breccias and climactic lag breccias: The 184 ka Lower Pumice 1 eruption sequence, Santorini, Greece. *Journal of Volcanology and Geothermal Research*, *324*, 200–219. <https://doi.org/10.1016/j.jvolgeores.2016.05.013>
- Smith, P. E., York, D., Chen, Y., & Evensen, N. M. (1996). Single crystal <sup>40</sup>Ar-<sup>39</sup>Ar dating of a Late Quaternary paroxysm on Kos, Greece: Concordance of terrestrial and marine ages. *Geophysical Research Letters*, *23*, 3037–3050. <https://doi.org/10.1029/96gl02759>
- Stewart, A. L., & McPhie, J. (2006). Facies architecture and Late Pliocene – Pleistocene evolution of a felsic volcanic island, Milos, Greece. *Bulletin of Volcanology*, *68*, 703–726. <https://doi.org/10.1007/s00445-005-0045-2>
- Tibaldi, A., Pasquare, F. A., Papanikolaou, D., & Nomikou, P. (2008). Tectonics of Nisyros Island, Greece, by field and offshore data, and analogue modelling. *Journal of Structural Geology*, *30*, 1489–1506. <https://doi.org/10.1016/j.jsg.2008.08.003>
- Tomlinson, E. L., Kinvig, H. S., Smith, V. C., Blundy, J. D., Gottsmann, J., Müller, W., & Menzies, M. A. (2012). The Upper and Lower Nisyros Pumices: Revisions to the Mediterranean tephratigraphic record based on micron-beam glass geochemistry. *Journal of Volcanology and Geothermal Research*, *243–244*, 69–80. <https://doi.org/10.1016/j.jvolgeores.2012.07.004>

- Tomlinson, E. L., Smith, V. C., Albert, P. G., Aydar, E., Civetta, L., Cioni, R., et al. (2015). The major and trace element glass compositions of the productive Mediterranean volcanic sources: Tools for correlating distal tephra layers in and around Europe. *Quaternary Science Reviews*, *118*, 48–66. <https://doi.org/10.1016/j.quascirev.2014.10.028>
- Tryon, C. A., Logan, M. A. V., Mouralis, D., Kuhn, S., Slimak, L., & Balkan-Atli, N. (2009). Building a tephrostratigraphic framework for the Paleolithic of Central Anatolia, Turkey. *Journal Archaeology Science*, *36*, 637–652. <https://doi.org/10.1016/j.jas.2008.10.006>
- Tyrlis, E., & Lelieveld, J. (2013). Climatology and dynamics of the summer etesian winds over the Eastern Mediterranean. *Journal of the Atmospheric Sciences*, *70*, 3374–3396. <https://doi.org/10.1175/JAS-D-13-035.1>
- Ulvrova, M., Paris, R., Nomikou, P., Kelfoun, K., Leibrandt, S., Tappin, D. R., & McCoy, F. W. (2016). Source of the tsunami generated by the 1650 AD eruption of Kolumbo submarine volcano (Aegean Sea, Greece). *Journal of Volcanology and Geothermal Research*, *321*, 125–139. <https://doi.org/10.1016/j.jvolgeores.2016.04.034>
- van Achterberg, E., Ryan, C. G., Jackson, S. E., & Griffin, W. (2001). Data reduction software for LA-ICP-MS: Appendix. In P. J. Sylvester (Ed.), *Laser ablation: ICP-mass spectrometry in the earth sciences: Principles and applications*. Mineralogical Association of Canada Short Course Series (Vol. 29, pp. 239–243). Mineralogical Association of Canada.
- Vespa, M., Keller, J., & Gertisser, R. (2006). Inter-Plinian explosive activity of Santorini volcano (Greece) during the past 150,000 years. *Journal of Volcanology and Geothermal Research*, *153*, 262–286. <https://doi.org/10.1016/j.jvolgeores.2005.12.009>
- Vinci, A. (1985). Distribution and chemical composition of tephra layers from Eastern Mediterranean abyssal sediments. *Marine Geology*, *64*, 143–155. [https://doi.org/10.1016/0025-3227\(85\)90165-3](https://doi.org/10.1016/0025-3227(85)90165-3)
- Volentik, A., Vanderkluisen, L., & Principe, C. (2002). Stratigraphy of the caldera walls of Nisyros volcano, Greece. *Eclogae Geologicae Helveticae*, *95*, 223–235.
- Vougioukalakis, G. E., & Fytikas, M. (2005). Volcanic hazards in the Aegean area, relative risk evaluation, monitoring and present state of the active volcanic centers. In M. Fytikas, & G. E. Vougioukalakis (Eds.), *The south Aegean active volcanic arc* (pp. 161–183). Elsevier. [https://doi.org/10.1016/s1871-644x\(05\)80037-3](https://doi.org/10.1016/s1871-644x(05)80037-3)
- Wegwerth, A., Dellwig, O., Wulf, S., Plessen, B., Kleinhanns, I., Nowaczyk, N. R., et al. (2019). Major hydrological shifts in the Black Sea “Lake” in response to ice sheet collapses during MIS 6 (130–184 ka BP). *Quaternary Science Reviews*, *219*, 126–144. <https://doi.org/10.1016/j.quascirev.2019.07.008>
- Wulf, S., Keller, J., Paterne, M., Mingram, J., Lauterbach, S., Opitz, S., et al. (2012). The 100–133 ka record of Italian explosive volcanism and revised tephrochronology of Lago Grande di Monticchio. *Quaternary Science Reviews*, *58*, 104–123. <https://doi.org/10.1016/j.quascirev.2012.10.020>
- Wulf, S., Keller, J., Satow, C., Gertisser, R., Kraml, M., Grant, K. M., et al. (2020). Advancing Santorini’s tephrostratigraphy: New glass geochemical data and improved marine-terrestrial tephra correlations for the past ~360 kyrs. *Earth-Science Reviews*, *200*, 102964. <https://doi.org/10.1016/j.earscirev.2019.102964>
- Wulf, S., Kraml, M., Brauer, A., Keller, J., & Negendank, J. F. W. (2004). Tephrochronology of the 100 ka lacustrine sediment record of Lago Grande di Monticchio (southern Italy). *Quaternary International*, *122*, 7–30. <https://doi.org/10.1016/j.quaint.2004.01.028>
- Wulf, S., Kraml, M., & Keller, J. (2008). Towards a detailed distal tephrostratigraphy in the Central Mediterranean: The last 20,000 yrs record of Lago Grande di Monticchio. *Journal of Volcanology and Geothermal Research*, *177*, 118–132. <https://doi.org/10.1016/j.jvolgeores.2007.10.009>
- Wulf, S., Kraml, M., Kuhn, T., Schwarz, M., Inthorn, M., Keller, J., et al. (2002). Marine tephra from the Cape Riva eruption (22 ka) of Santorini in the Sea of Marmara. *Marine Geology*, *183*, 131–141. [https://doi.org/10.1016/s0025-3227\(01\)00302-4](https://doi.org/10.1016/s0025-3227(01)00302-4)
- Zhou, X., Kuiper, K., Wijbrans, J., Boehm, K., & Vroon, P. (2021). Eruptive history and 40Ar/39Ar geochronology of the Milos volcanic field, Greece. *Geochronology*, *3*, 273–297. <https://doi.org/10.5194/gchron-3-273-2021>
- Zhu, L., Mitchell, B. J., Akyol, N., Cemen, I., & Kekovali, K. (2006). Crustal thickness variations in the Aegean region and implications for the extension of continental crust. *Journal of Geophysical Research*, *111*. <https://doi.org/10.1029/2005JB003770>